# Kv2 subunits underlie slowly inactivating potassium current in rat neocortical pyramidal neurons

D. Guan[1], T. Tkatch[2], D. J. Surmeier[2], W. E. Armstrong[1] and R. C. Foehring[1]

[1]*Department of Anatomy and Neurobiology, University of Tennessee, 855 Monroe Avenue, Memphis, TN 38163, USA*
[2]*Department of Physiology, Northwestern University, 745 N. Fairbanks Court, Chicago, IL 60611, USA*

**We determined the expression of Kv2 channel subunits in rat somatosensory and motor cortex and tested for the contributions of Kv2 subunits to slowly inactivating $K^+$ currents in supragranular pyramidal neurons. Single cell RT-PCR showed that virtually all pyramidal cells expressed Kv2.1 mRNA and ∼80% expressed Kv2.2 mRNA. Immunocytochemistry revealed striking differences in the distribution of Kv2.1 and Kv2.2 subunits. Kv2.1 subunits were clustered and located on somata and proximal dendrites of all pyramidal cells. Kv2.2 subunits were primarily distributed on large apical dendrites of a subset of pyramidal cells from deep layers. We used two methods for isolating currents through Kv2 channels after excluding contributions from Kv1 subunits: intracellular diffusion of Kv2.1 antibodies through the recording pipette and extracellular application of rStromatoxin-1 (ScTx). The Kv2.1 antibody specifically blocked the slowly inactivating $K^+$ current by 25–50% (at 8 min), demonstrating that Kv2.1 subunits underlie much of this current in neocortical pyramidal neurons. ScTx (300 nM) also inhibited ∼40% of the slowly inactivating $K^+$ current. We observed occlusion between the actions of Kv2.1 antibody and ScTx. In addition, Kv2.1 antibody- and ScTx-sensitive currents demonstrated similar recovery from inactivation and voltage dependence and kinetics of activation and inactivation. These data indicate that both agents targeted the same channels. Considering the localization of Kv2.1 and 2.2 subunits, currents from truncated dissociated cells are probably dominated by Kv2.1 subunits. Compared with Kv2.1 currents in expression systems, the Kv2.1 current in neocortical pyramidal cells activated and inactivated at relatively negative potentials and was very sensitive to holding potential.**

(Resubmitted 17 January 2007; accepted after revision 15 March 2007; first published online 22 March 2007)
**Corresponding author** R. C. Foehring: Department of Anatomy and Neurobiology, University of Tennessee, 855 Monroe Avenue, Memphis, TN 38163, USA. Email: rfoehrin@utmem.edu

Voltage-gated potassium channels (Kv) are extremely diverse, with 12 known subfamilies of Kv channels (Coetzee *et al.* 1999). They play pivotal roles in regulating neuronal excitability, shaping action potentials, and modulating spike patterns (Hille, 2000). Relationships between specific channel subunits and native potassium currents are poorly understood, however. Channel subunits responsible for voltage-gated potassium currents in neurons have been identified in very few cases (e.g. Wang *et al.* 1998; Murakoshi & Trimmer, 1999; Du *et al.* 2000; Malin & Nerbonne, 2002; Yuan *et al.* 2005). Knowledge of such molecular correlations is needed to understand modulation of $K^+$ currents by neurotransmitters and $K^+$ channel-related pathophysiology (cf. McCormick *et al.* 1993; Wible *et al.* 1997; Wickenden, 2002).

On the basis of biophysical properties (especially inactivation kinetics) and sensitivity to TEA and 4-AP, voltage-gated $K^+$ currents in pyramidal neurons are typically divided into $I_A$, $I_M$, $I_K$, and $I_D$ (Storm, 1990; Zhou & Hablitz, 1996; Locke & Nerbonne, 1997; Bekkers, 2000*a*,*b*; Korngreen & Sakmann, 2000). $I_A$ is a rapidly activating, rapidly inactivating current. $I_M$ is a very slowly activating and deactivating and non-inactivating current that is highly sensitive to muscarinic agonists (Brown & Adams, 1980). $I_D$ was originally described as a slowly inactivating, 4-AP-sensitive current that was very sensitive to holding potential (Storm, 1988). The most common current definition of $I_D$ is the current sensitive to $\alpha$-dendrotoxin ($\alpha$-DTX; Wu & Barish, 1992; Bekkers, 2000*a*,*b*; Korngreen & Sakmann, 2000; reviewed in Guan *et al.* 2006). $I_K$ is also referred to as the delayed rectifier current ($I_{DR}$: Zhou & Hablitz, 1996). This slowly inactivating current activates more slowly than $I_A$ and $I_D$ but more rapidly than $I_M$ and is variably TEA sensitive.

Classification of $K^+$ currents on the basis of biophysics and/or TEA and 4-AP sensitivities has

 DOI: 10.1113/jphysiol.2007.128454

proven unsatisfactory for many reasons. Besides the differing definitions of $I_D$, the slowly inactivating current has complicated kinetics, voltage dependence and pharmacology (Foehring & Surmeier, 1993). A more natural classification system is preferable, based upon the underlying channel subunits.

Expression of Kv subunits in expression systems has revealed a great deal about the properties of specific subunits but we have only limited knowledge of the contributions of these subunits to currents in native neuronal membranes. We previously used single cell RT-PCR, immunocytochemistry, and recordings with specific peptide toxins to demonstrate that layer II/III pyramidal cells express several Kv1 subunits (Kv1.1–1.4: Guan *et al.* 2006). $\alpha$-DTX blocks channels containing Kv1.1, 1.2 and 1.6 subunits. The $\alpha$-DTX-sensitive current made up ∼10% of the slowly inactivating current from negative holding potentials (Guan *et al.* 2006). What channel subunits underlie the remaining 90% of the current? Two major candidates are Kv2 and Kv7 family subunits.

In sympathetic neurons, $I_M$ is due to heteromultimeric expression of Kv7 subunits (Wang *et al.* 1998; Selyanko *et al.* 2002; Shah *et al.* 2002). Kv2.1 is ubiquitously expressed throughout the mammalian brain with the most abundant expression on somata and proximal dendritic processes of pyramidal cells in cerebral cortex and hippocampus (Frech *et al.* 1989; Trimmer, 1991; Hwang *et al.* 1993; Du *et al.* 1998). In cultured hippocampal pyramidal neurons, the sustained outward potassium current is greatly reduced by intracellular diffusion of polyclonal Kv2.1 antibodies or by antisense treatment against Kv2.1, indicating that Kv2.1 is a major contributor to the delayed rectifier currents (Murakoshi & Trimmer, 1999: Du *et al.* 2000). Intracellular application of the Kv2.1 antibody also demonstrated Kv2.1 involvement in smooth muscle (Archer *et al.* 1998; Lu *et al.* 2002). Transient over-expression of dominant-negative Kv2 subunits in embryonic or perinatal neurons demonstrated that native Kv2 subunits contribute to the sustained or slowly activating potassium currents in many cell types (e.g. Kv2.2 in spinal neurons: Blaine & Ribera, 2001; Kv2.1 and Kv2.2 in rat superior cervical ganglion sympathetic neurons: Malin & Nerbonne, 2002; Kv2.1 in pancreatic $\beta$ cells: MacDonald *et al.* 2002). We hypothesized that Kv2 channels underlie most of the slowly inactivating potassium current in layer II/III neocortical pyramidal neurons.

We found expression of Kv2.1 and Kv2.2 mRNA and channel proteins in neocortical pyramidal neurons. We isolated currents through Kv2 channels by including Kv2.1 antibodies in the recording pipette and by extracellular administration of a peptide gating modifier of Kv2, rStromatoxin-1 (ScTx: Escoubas *et al.* 2002). The Kv2.1-mediated current was the dominant current in layer II/III pyramidal cells. We characterized the biophysical properties of these currents.

## Methods

### Tissue preparation

These studies were performed on juvenile rats (Sprague–Dawley, postnatal day 16–42 (P16–42)). All procedures were approved by the Animal Care and Use Committee, University of Tennessee, Health Science Center. Briefly, the animal was placed into a sealed plastic container into which gauze soaked with isofluorane was placed under a fibreglass screen floor. The animals were anaesthetized with isofluorane until the animal was areflexive. After anaesthesia with isoflurane, the animals were decapitated and the brain was removed and held in ice-cold cutting solution for 30–60 s. The cutting solution contained (mM): 250 sucrose, 25 KCl, 1 $NaH_2PO_4$, 11 glucose, 4 $MgSO_4$, 0.1 $CaCl_2$, 15 Hepes (pH 7.3–7.4; 300 mosmol $l^{-1}$). Coronal slices 400 $\mu$m thick of the fronto-parietal regions were cut using a vibrating tissue slicer (World Precision Instruments, Sarasota, FL, USA). The slices were then transferred to a mesh surface in a chamber containing artificial cerebrospinal fluid (aCSF), which was continuously bubbled with a 95% $O_2$–5% $CO_2$ (carbogen) mixture at room temperature (RT). The aCSF contained (mM): 125 NaCl, 3 KCl, 2 $CaCl_2$, 2 $MgCl_2$, 1.25 $NaH_2PO_4$, 26 $NaHCO_3$, and 20 glucose (pH 7.4; 310 mosmol $l^{-1}$).

### Acute isolation of neurons

The supragranular layers (I–III) or deep layers (V/VI) of primary motor and primary somatosensory cortex were dissected into 3-mm-wide pieces from brain slices under a stereomicroscope. Four to ten tissue pieces were then transferred to oxygenated aCSF (35°C) with added enzyme (Sigma Protease type XIV, 1.2 mg $ml^{-1}$: Sigma Chemicals, St Louis, MO, USA). After 12–30 min of incubation in enzyme, the tissue pieces were washed with sodium isethionate solution, which consisted of (mM): 140 sodium isethionate, 2 KCl, 4 $MgCl_2$, 23 glucose, 15 Hepes (pH 7.3; 300 mosmol $l^{-1}$). This solution and enzyme-treated tissue pieces were triturated using three successively smaller fire-polished pipettes to release individual neuronal somata. The supernatant from each trituration step was collected and transferred to a fresh container and plated onto a plastic Petri dish (Nunc, Rochester, NY, USA) on an inverted microscope stage. After 5–8 min of settling time, a uniform background flow of ∼1 ml $min^{-1}$ of Hepes-buffered saline solution (HBSS) was established. HBSS consisted of (mM): 138 NaCl, 3 KCl, 1 $MgCl_2$, 2 $CaCl_2$, 10 Hepes, 10–20 dextrose (pH 7.3; 300–305 mosmol $l^{-1}$).

### Electrophysiology

Whole cell patch clamp recordings were performed on 110 acutely dissociated pyramidal neurons (56 from P27–P36, 43 from P21–P26, 11 from P16–P20). A multibarrel array of glass capillaries (500 $\mu$m outer diameter) was used to apply external recording solutions. Solutions were changed by moving the active barrel (from which the solution flows) to surround the recorded cell. To isolate $K^+$ current for recording, the external solution contained (mM): 140 sodium isethionate, 3 KCl, 1 $MgCl_2$, 12 glucose, 10 Hepes, and 1.5 $CaCl_2$, plus 1 $\mu$M tetrodotoxin (TTX) and 100–400 $\mu$M $CdCl_2$ for blocking $Na^+$ and $Ca^{2+}$ channels, respectively. A few experiments were performed in the absence of $Cd^{2+}$, to test for its effects on $K^+$ current components. The following peptide toxins were used individually or jointly in the external solution for blocking specific Kv channels: $\alpha$-dendrotoxin ($\alpha$-DTX: 100–200 nM to block Kv1.1, 1.2 and 1.6), rMargatoxin (MTX: 10–20 nM to block Kv1.3), and rStromatoxin-1 (ScTx: 100–1000 nM to block Kv2.1, Kv2.2 and Kv4.2). BSA (0.1%) was added to all solutions to prevent peptides from binding to glass and plastic vessels. All peptide toxins were obtained from Alomone Laboratories (Alomone Laboratories, Ltd, Jerusalem, Israel). In some experiments, TEA was included in external solutions, with the concentration of sodium isethionate accordingly reduced to maintain an osmolality of 300 mosmol $l^{-1}$.

Recordings were made with a DAGAN 8900 (Minneapolis, MN, USA) amplifier at room temperature (21–23°C). Corning 7052 capillary glass (Garner Glass: Claremont, CA, USA) was used to create electrodes on a Sutter Instruments (Novato, CA, USA) Model P-87 Flaming/Brown micropipette puller. Electrodes were fire-polished and filled with internal solution. The internal solution consisted of (mM): 86 $KMeSO_4$, 54 KOH, 2 $MgCl_2$, 40 Hepes, 2 adenosine triphosphate disodium (ATP), 0.2 guanosine 5′-triphosphate sodium salt (GTP), 9 creatine phosphate, 0.1 leupeptin, 10 BAPTA (pH 7.2; 270 mosmol $l^{-1}$). Electrode resistances were 1.4–2.2 MΩ. Series resistance was usually compensated by 70–90%. Cells with calculated series resistance errors of $> 5$ mV were discarded (series resistance error (mV) = series resistance after compensation (GΩ) multiplied by peak current (pA)). Membrane potentials were corrected for the measured liquid junctional potential (+8 mV). Data acquisition (20 kHz sampling, filtered at 5 kHz) and analysis were done using pCLAMP 8 software (Axon Instruments, Union City, CA, USA) and Prism 4 (GraphPad Software, Inc., San Diego, CA, USA). Linear leak currents and capacitative artifacts were subtracted using an online *P*/4 or *P*/6 protocol.

For the experiments using intracellular antibodies, the pipettes were dipped in an antibody-free internal solution and then back filled with the internal solution containing the antibodies of interest. We applied monoclonal and polyclonal antibodies to the Kv2.1 C-terminus (monoclonal: AAs 509–853; polyclonal: AAs 837–853: Trimmer, 1991; Misonou *et al.* 2005) intracellularly to 49 cells (6 cells: P16–P20, 43 cells P21–33). Polyclonal antibodies were obtained from Alamone Laboratories. Monoclonal Kv2.1 antibodies were initially obtained from Upstate, and more recently from Neuromab (Davis, CA, USA). Similar results were obtained with both polyclonal and monoclonal antibodies from all of these sources. Kv2.1 antibody concentration in the internal solution was 8–10 $\mu$g ml$^{-1}$ or 0.4 $\mu$g ml$^{-1}$. In control experiments, Kv2.1 antibodies were first mixed with Kv2.1 antigens of the same concentration. After 1 h incubation at room temperature, neutralized Kv2.1 antibodies were added to the internal solution for recording. Effects of polyclonal antibodies to the C-terminus of Kv2.2 (Blaine & Ribera, 1998; obtained from Phosphosolutions: Colorado Biosciences Park, Aurora, CO, USA) were tested in the internal solution at concentration of 1 : 100.

### Single cell RT-PCR

Acutely dissociated neurons (layers I–III or V/VI) were harvested for these experiments (9 animals: P28–P37). Pyramidal neurons were identified by shape and the presence of an apical dendrite. Electrode glass (Corning 7052) was autoclaved and heated to 150–200°C for 2 h. After formation of a giga-ohm seal, the cell was lifted up into a stream of HBSS flowing out of the multibarrel array. Suction was increased to aspirate the cell into the pipette. The pipette contained diethylpyrocarbonate-treated (DEPC) water and 0.8 U ml$^{-1}$ Superase-In (Ambion, Austin, TX, USA). After aspiration, the pipette tip containing the cell was broken into a 0.6 ml pre-siliconized Midwest Scientific tube (Valley Park, MO, USA) and the contents ejected into the cell collection components for reverse transcription. Eppendorf tubes containing 0.7 $\mu$l of SUPERase-In (20 mg $l^{-1}$), 1.9 $\mu$l of diethylpyrocarbonate-treated water, 1 $\mu$l of dNTPs (10 mM), 0.7 $\mu$l of BSA (143 mg $l^{-1}$) and 0.7 $\mu$l of oligo-dT (0.5 mg $l^{-1}$) together with cell contents were heated to 65°C for 5 min and then placed on ice for at least 1 min. Single-strand cDNA was synthesized from the cellular mRNA by adding 2 $\mu$l of 10× PCR buffer, 4 $\mu$l of $MgCl_2$ (25 mM), 2 $\mu$l of DTT (0.1 M), 1 $\mu$l of RNase out (40 mg $l^{-1}$), 1 $\mu$l of Superscript III (50 $\mu$g $\mu$l$^{-1}$) and 6 $\mu$l of diethylpyrocarbonate-treated water to the cell. The reverse transcriptase was then incubated at 50°C for 90 min. The reaction was terminated by heating the mixture to 85°C for 5 min. The RNA strand in the RNA–DNA hybrid was then removed by adding 0.5 $\mu$l of RNase H (2 $\mu$g ml$^{-1}$) and incubated at 37°C for 20 min. All reagents except SUPERase-In were

obtained from Invitrogen (Gaithersburg, MD, USA). PCR was performed using procedures designed to minimize cross contamination. Negative controls for contamination from extraneous (replace cellular template with water) and genomic DNA (without reverse transcriptase) were run for every batch of neurons. The single cell cDNA generated from the above step was subjected to conventional PCR using a programmable thermal cycler. PCR primers were developed from the GenBank sequences with OLIGO software (v6.6). Primers were for calcium calmodulin kinase II (CamKII), Kv2.1 and Kv2.2 (Baranauskas *et al.* 1999; Guan *et al.* 2006). 'Touchdown' protocols were implemented for more efficient amplification of single cell DNA: 35 cycles were run at the optimal annealing temperature for each primer set, then the annealing temperature was decreased by 1°C for two cycles, five times, for a total of 45 cycles.

### Immunocytochemistry

Animals ($n = 8$, P26–P42) were anaesthetized with sodium pentobarbital (50 mg kg$^{-1}$ I.P.). The anaesthetized animals were transcardially perfused with 0.01 M sodium phosphate buffer plus 0.89% NaCl (PBS) followed by PBS-buffered 4% paraformaldehyde and 0.2% picric acid. Brains were removed, post-fixed for ∼12 h at 4°C, then blocked and placed in a solution of fixative containing sucrose (30% w/v) for cryoprotection. Sections through the cortex were taken at 40 $\mu$m on a freezing microtome, rinsed in PBS, and incubated in 2% normal goat serum with 3% $H_2O_2$ for 1–2 h to reduce background staining. Antibodies to Kv2.2 subunits were obtained from PhosphoSolutions (Kv2.2; Aurora) or donated by Dr A. Ribera (University of Colorado, Denver). Similar results were obtained with polyclonal (Sigma: $n = 2$) and monoclonal antibodies (Upstate (Billerica, MA, USA: $n = 2$) or NeuroMab (UC Davis, CA, USA: $n = 4$)) to Kv2.1. These were the same antibodies as used for intracellular block of $K^+$ currents (see above). Antibodies were tested first at various concentrations (1 : 100 to 1 : 1000) in PBS and 0.5% Triton X-100 (PBS-TX).

### ABC staining

After three rinses with PBS-TX, the sections were incubated in biotinylated goat anti-rabbit (GAR-B) or horse anti-mouse (HAM-B) antibodies at 1 : 200 overnight (4°C). After three rinses in PBS-TX, the sections were incubated for ∼4 h with avidin–biotin–peroxidase (ABC: Vector Laboratories) dissolved in PBS-TX. After three rinses in PBS-TX, the sections were reacted (as per Vector protocol) with $Ni^{2+}$-intensified Diamino benzidine (DAB) (60 mg ml$^{-1}$) plus 0.003% $H_2O_2$ for 5–10 min. The reaction was terminated by several rinses in PBS-TX. The sections were then mounted on gelatin-coated glass slides, dehydrated, coverslipped, and viewed with conventional light microscopy.

### Immunofluorescence

Double staining was accomplished using the PhosphoSolutions polyclonal Kv2.2 antibody and the Neuromab monoclonal Kv2.1 antibody diluted in PBS-TX. Following overnight incubation with a cocktail of primary antibodies (1 : 200 to 1 : 400), the sections were incubated overnight in a cocktail of secondary antibodies (1 : 200) consisting of Fluorescein GAR-(FITC) and GOAT anti-mouse (GAM)-AlexaFluor 568 conjugates, all at 4°C. The sections were rinsed in PBS-TX, mounted on gelatin-coated slides, and coverslipped with Vectashield (Vector). These sections were viewed with a Bio-Rad (Hercules, CA, USA) confocal microscope equipped with a krypton–argon laser. FITC was examined with a 488 nm excitation filter (emission bandpass 522 nm), and AlexaFluor 568 was examined with a 568 nm excitation filter (emission bandpass 605 nm). The optical section thickness was 1–2 $\mu$m. Sections were viewed singly or in stacks of 5–12 sections using 40, 60 or 100× oil immersion objectives (n.a. 1.35, 1.4 and 1.4, respectively). Confocal images (1024 × 1024 pixels) were acquired as 24-bit colour images and viewed with ImageJ (NIH) software. The final confocal figures were made in Adobe Photoshop, with minimal alteration in dynamic range.

### Electron microscopy

For electron microscopy, we used the fixative described above with an additional 0.25–0.5% glutaraldehyde. The brains were sectioned at 50 $\mu$m on a vibrating microtome (Leica 1000) into PBS, and no Triton X-100 was used for these protocols. After rinsing, the sections were pre-treated with 0.5% $H_2O_2$ and 1% sodium borohydride to reduce background staining. Following the reaction, sections were reacted with 1% osmium in PBS for 1 h. Osmicated sections were dehydrated, stained *en bloc* with 2% uranyl acetate, and embedded in plastic (Spurr's resin, EMS, Fort Washington, PA, USA). Ultrathin (75–80 nm) sections were contrasted with lead citrate and uranyl acetate and viewed at 60–100 kV on a JEOL 2000 transmission electron microscope. With the same ABC localization method described above, penetration of antibodies on the Vibratome section without detergent was less than 5 $\mu$m. Digital images (2240 × 2944 pixels) were acquired directly with a Hamamatsu ORCA camera and AMT Advantage (Danvers, MA, USA) software. The final electron microscopic figures were made in Adobe Photoshop, with minimal alteration in dynamic range.

### Statistics

Data are presented as mean ± standard error of the mean (s.e.m.). Prism Software (GraphPad, Software, Inc., San Diego, CA, USA) was used for statistical tests of significance. Paired or unpaired *t* tests were used to compare sample population data throughout. *P* values $< 0.05$ were considered to be significantly different. Multiple comparisons used one-way ANOVA with Tukey's multiple comparison test for *post hoc* comparison of means. Sample population data are represented as scatter plots or as box plots (Tukey, 1977). Box plots indicate the upper and lower quartiles as edges of the box, with the median represented as a line crossing the box. The stems indicate the largest and smallest non-outlying values, and outliers are indicated by open circles. Outlying values are greater than 1.5 times the quartile boundaries.

## Results

### Kv2.1 mRNA and Kv2.2 mRNA were expressed in pyramidal cells

Single cell RT-PCR experiments were performed to determine whether pyramidal cells expressed Kv2.1 or Kv2.2 mRNA (9 animals, P28–P37). A primer for $Ca^{2+}$ calmodulin kinase II (CamKII), a specific marker of pyramidal cells in cortex (Jones *et al.* 1994), was used to confirm the identity of the neurons as pyramidal (Fig. 1). All cells were CamKII positive. In layers II/III, Kv2.1 mRNA was detected in 52/53 (98%), and Kv2.2 mRNA was detected in 42/53 cells (79%, Fig. 1*B*). In deep layer pyramidal neurons (V/VI), Kv2.1 mRNA was detected in 17/20 cells (85%) and Kv2.2 mRNA detected in 12/20 (60%, Fig. 1*B*).

### Kv2.1 channels were localized to soma/proximal dendrites and Kv2.2 channels to dendrites

The mRNA data indicated that virtually all pyramidal cells express Kv2.1 mRNA and most express Kv2.2 mRNA. We next used immunocytochemistry to determine whether the corresponding proteins were expressed and if so, in which cell compartments. Kv2.1 subunits were arranged in variably sized clusters on somata and proximal dendrites of the pyramidal cells in both layers II/III (Fig. 2*D*, stained green) and layer V (Fig. 2*A*, stained green). In contrast, Kv2.2 proteins were mostly confined to large apical dendrites of a subset of the pyramidal cells in deep layers (Fig. 2*B* and *D*, stained red). We were able to connect layer 5 somata with Kv2.2-immunopositive dendrites in many cases, but not layer 2/3 somata (Fig. 2*C* and *D*). Little somatic staining was evident in either layer. Electron microscopy indicated that Kv2.2 subunits were found in dendrites and dendritic spines (Fig. 2*E*). The bulk of the Kv2.2 staining was not associated with the plasma membrane, but rather appeared distributed in vesicular profile throughout the dendrites (Fig. 2*F*).

### The major outward $K^+$ current was sensitive to TEA and holding potential

We previously found that ∼10% of the slowly inactivating current was due to Kv1 subunits (Guan *et al.* 2006). We now address which subunits underlie the bulk of the current. In all experiments, $\alpha$-DTX and MTX were added to the external solutions to block the Kv1 current. Every 10 s, transmembrane potential was stepped to +10 mV for 200 ms from the holding potential. We determined the TEA dose–response relationship at holding potentials of −80 and −40 mV in the same cell ($n = 6$, P21–P30). $K^+$ currents were tested after the amplitude of the $K^+$ currents was stable. Relative block of the current by TEA (at 200 ms) was calculated and was used for fitting the following dose–response curve:

$$I_{max} - I/I_{max} = \{B_{max}/1 + \exp[2.3\log(dose)]/IC_{50}\}^{n_H}$$

where $I_{max}$ is the largest current at 200 ms in the control solution, $n_H$ is the Hill coefficient, and $B_{max}$ represents the maximum relative block.

As shown in Fig. 3*A*, almost all of the slowly inactivating current was TEA sensitive. The TEA-sensitive current activated and inactivated slowly. From the −80 mV

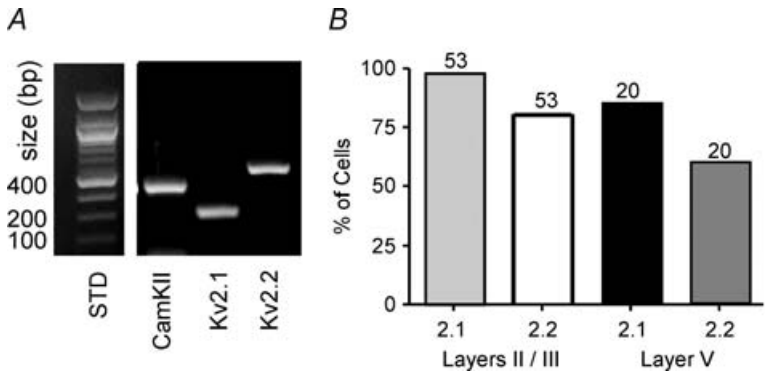


**Figure 1. Single cell RT-PCR**
*A*, gel for a single layer II/III pyramidal cell from a P28 rat. This cell expressed mRNA for CamKII (marker for pyramidal cells), Kv2.1 and Kv2.2. STD, standards. *B*, histograms to show population data for Kv2 mRNA. Numbers above bars = number of cells. Virtually all pyramidal cells express mRNA for Kv2.1 and most for Kv2.2.

holding potential, the $IC_{50}$ for TEA was 10.3 mM (Fig. 3*B*). When holding potential was increased to −40 mV, 93% of the outward $K^+$ current was inactivated (Fig. 3*C*). The remaining current demonstrated high TEA sensitivity ($IC_{50} = 1.5$ mM, Fig. 3*D*). Therefore, the major outward $K^+$ current in the pyramidal cells was TEA sensitive and very sensitive to holding potential (cf. Foehring & Surmeier, 1993).

To eliminate $Ca^{2+}$ and $Ca^{2+}$-dependent currents, we recorded in the presence of extracellular $Cd^{2+}$. This divalent ion has been shown to alter voltage dependence of transient (Song *et al.* 1998; Wickenden *et al.* 1999) and delayed rectifier (Follmer *et al.* 1992; Davidson & Kehl, 1995) $K^+$ channels. Therefore, we compared currents in 100–400 $\mu$M $Cd^{2+}$-containing and $Cd^{2+}$-free solutions ($n = 5$ cells, P28–P30). These cells expressed rapidly inactivating (A current) and slowly inactivating components in the absence of $Cd^{2+}$. In all cells, the transient A component was reduced by 40–90% by $Cd^{2+}$ ($77 \pm 4\%$ at −10 mV: Fig. 3*E*). The steady-state current was blocked $15 \pm 3\%$ at −10 mV ($13.5 \pm 4\%$ at +10 mV: Fig. 3*E*). In four cells we examined the effects of $Cd^{2+}$ on steady-state activation of the slowly inactivating component (measured at 200 ms: Fig. 3*E* and *F*). $Cd^{2+}$ had little effect on the voltage dependence of the slowly inactivating component ($V_{1/2}$ was $-3.6 \pm 3.0$ mV in control and $-1.4 \pm 3.5$ mV in $Cd^{2+}$), consistent with previous results in medium spiny neurons (Song *et al.* 1998).

### Intracellular diffusion of Kv2.1 antibodies inhibited a slowly inactivating $K^+$ current

To test whether Kv2.1 subunits underlie the slowly inactivating current, we recorded outward currents under four intracellular conditions: control (without Kv2.1 antibody in the pipette: P21–P30), intracellular anti-Kv2.1 (diluted 1 : 100 for a final concentration of 10 $\mu$g ml$^{-1}$: P21–P32), neutralized anti-Kv2.1 (1 : 1 antibody to antigen, see Methods: P15–P27), and anti-Kv2.2 (10 $\mu$g ml$^{-1}$: P21–P33). In most cases, we used the rabbit

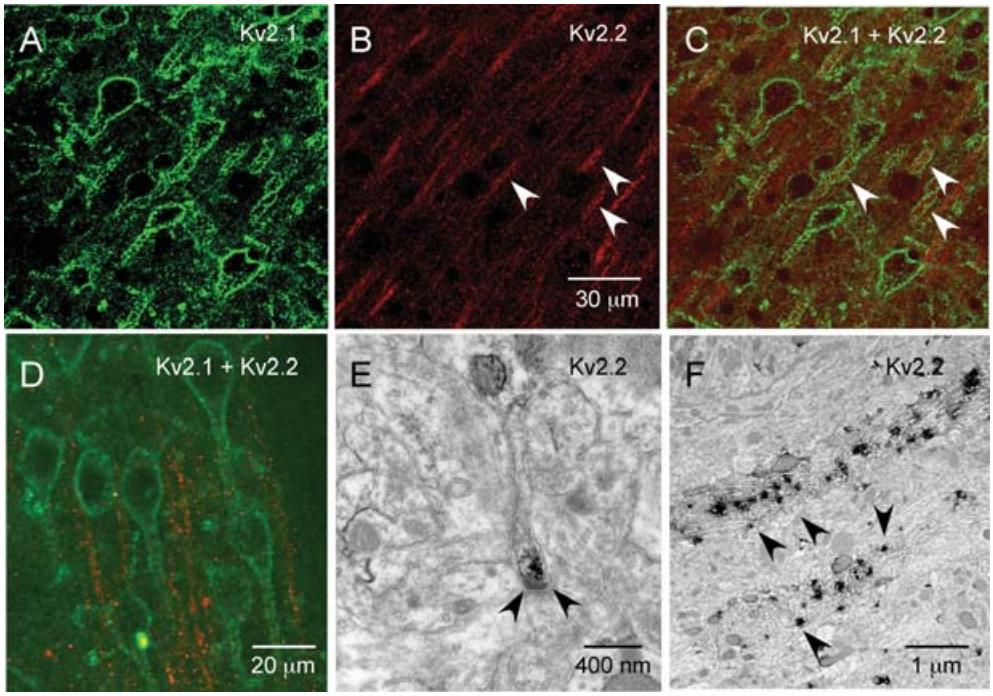


**Figure 2. Localization of Kv2.1 and Kv2.2 subunits**
*A–C*, layer V of somatosensory cortex (P35 rat). Scale bar in *B* refers to *A–C*. *A*, confocal image of single 1 $\mu$m section with fluorescent staining for monoclonal anti-Kv2.1 (Neuromab: green). Kv2.1 is patchy and distributed on somata and proximal apical dendrites (mostly < 50 $\mu$m from soma) of all pyramidal cells. *B*, polyclonal anti-Kv2.2 (Phosphosolutions: red) Note Kv2.2 is largely restricted to large dendritic shafts. Arrows point out the same dendrites indicated by arrows in *C*. *C*, superimposed Kv2.1 and Kv2.2. In a few cases, Kv2.2-positive (red) dendrites are in continuity with Kv2.1-positive (green) dendrites (e.g. arrows). *D*, layer 3 of somatosensory cortex (different P35 animal). Confocal image of single 1 $\mu$m section with superimposed fluorescent staining for monoclonal anti-Kv2.1 (green) and polyclonal anti-Kv2.2 (red). Kv2.2 stains some dendrites, which are *en passant* from deeper layers (we could not match layer 3 pyramidal cell somata with anti-Kv2.2-stained dendrites). Scale bar = 20 $\mu$m. *E*, EM image of Kv2.2 localization in dendritic spine (between arrows). *F*, at the EM level, much of the Kv2.2 staining was within the cytoplasm of pyramidal cell apical dendrites. The staining appeared vesicular (e.g. arrows).

polyclonal antibody (Alamone: $n = 8$ cells: P21–P32), which blocked $38 \pm 7\%$ at 8 min. Similar results were obtained with the monoclonal antibody ($30 \pm 6\%$: $n = 3$; P27–P28; Neuromab, Upstate) to the C-terminus. Currents were recorded every 10–30 s using the voltage protocol shown in the lower part of Fig. 4*B*. Currents were normalized to the amplitude of the initial sweep. The average current in the control ($n = 9$ cells) and the neutralized-antibody groups ($n = 7$) changed little over 8 min. In 6 of 16 of these cells, run-up of current ($< 20\%$) was observed in the initial 3–7 min, followed by current run-down. In our previous paper (Guan *et al.* 2006), we reported that after an initial stable period, average run-down rate was $87 \pm 21$ pA min$^{-1}$ ($n = 18$). It is notable that the run-down current in that study and in the present study activated much more slowly than the AB-sensitive current (e.g. Fig. 4*D*: initial current – current at 8 min). These data suggest that a different, slower current dominates run-down.

In contrast, diffusion of anti-Kv2.1 into the cell reduced the outward $K^+$ current by 25–50% at 8 min ($n = 11$; Fig. 4*A*). Figure 4*B* shows a typical example of the effects of anti-Kv2.1. Subtraction of the current at 8 min from the initial current revealed that the antibody-sensitive current was persistent and activated faster than the remaining current. Figure 4*C* summarizes the average current amplitude at 8 min for each group (normalized to the initial current amplitude). In the group with anti-Kv2.1 (combined mono- and polyclonal), $33 \pm 6\%$ of the outward $K^+$ current was reduced at 8 min (ANOVA: $P < 0.05$), compared with $8 \pm 8\%$ reduction in the group with neutralized anti-Kv2.1, and $4.0 \pm 5\%$ reduction in the control group. These data demonstrate that Kv2.1 subunits are a major contributor to the slowly inactivating current.

When Kv2.2 antibody was included in the pipette ($10\ \mu$g ml$^{-1}$), the amplitude of outward $K^+$ current declined by $7 \pm 9\%$ in 8 min ($n = 4$), similar to the results with neutralized anti-Kv2.1. These data suggest little Kv2.2 current in soma/proximal dendrites of these truncated, dissociated cells, consistent with our data for Kv2.2 distribution (Fig. 2).

## Steady-state activation of anti-Kv2.1-sensitive currents

We studied activation properties of the antibody-sensitive current in four cells with anti-Kv2.1 in the pipette ($10\ \mu$g ml$^{-1}$). We obtained data from a family of voltage steps to various potentials (Fig. 5). Figure 5*A* and *B* illustrate current recordings in one pyramidal cell (age: P20) at 0 and 6 min. As seen in Fig. 5*A*, initial currents were composed of an A-like, rapidly inactivating component and a slowly inactivating component. Under our recording conditions, transient A-type currents were observed in 80% of neurons from animals < P20 (8/10) and 22% from animals ≥ P27 (8/36). These data suggest developmental down-regulation of $I_A$, but the data are skewed by the presence of $Cd^{2+}$, which shifts the activation range for A currents to much more positive voltages (Davidson *et al.* 1995; Song *et al.* 1998). In cells with detectable A current,

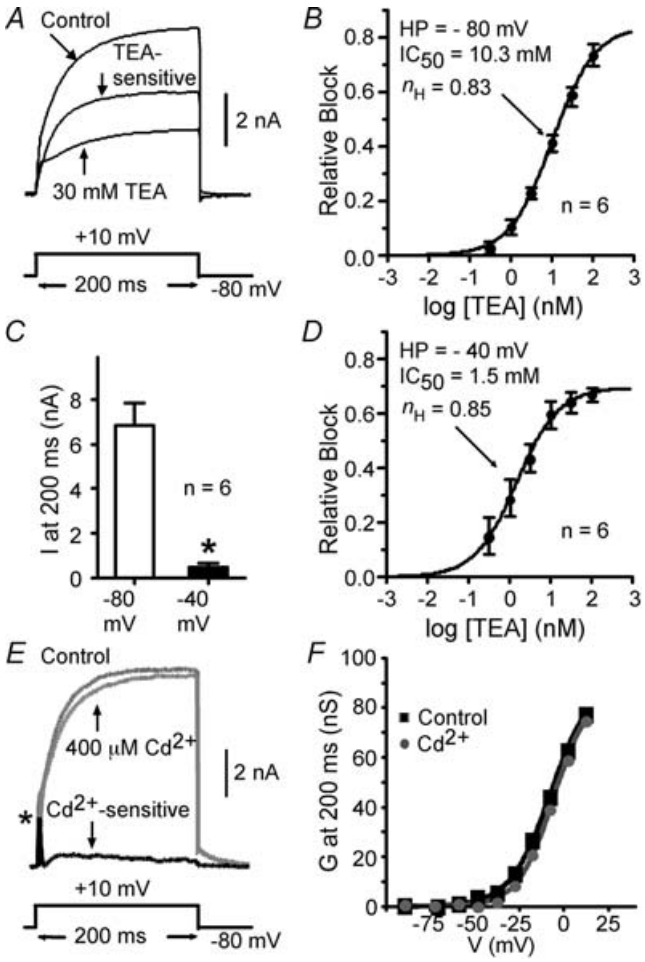


**Figure 3. TEA, $Cd^{2+}$ and holding potential sensitivities of the outward $K^+$ currents**

$\alpha$-DTX and MgTX were used in all external solutions to exclude the currents associated with Kv1 channels. Data are presented as mean ± S.E.M. *A*, example of the $K^+$ current recorded from a holding potential of − 80 mV. 30-mM TEA inhibited a large, slowly activating current component. *B*, the dose–response relationship for TEA inhibition from holding potential of −80 mV. Over 80% of the outward $K^+$ current was TEA sensitive, with an $IC_{50}$ of 10.3 mM. $n_H$, Hill coefficient. *C*, when the holding potential was changed to −40 mV from −80 mV, most outward $K^+$ current was inactivated. *Statistical significance ($P < 0.05$). *D*, from a holding potential of −40 mV, the small, non-inactivated, outward $K^+$ current was TEA sensitive, with an $IC_{50}$ of 1.5 mM. *E*, representative traces for currents in response to a voltage step to +10 mV in control solution ($Cd^{2+}$-free) and in the presence of 400 $\mu$M $Cd^{2+}$. The subtracted record (black trace) shows that the fast, transient A current (*) was almost eliminated while the slowly inactivating current was only modestly affected by $Cd^{2+}$. *F*, plot of conductance (*G*) at 200 ms *versus* the voltage step indicates that the voltage dependence of activation was little affected by $Cd^{2+}$ (grey trace; protocol as in Fig. 5*C*).

the slowly activating current was prominently inhibited by the Kv2.1 antibody, while the A current was unaffected (Fig. 5*B*). Figure 5*C* illustrates antibody-sensitive currents obtained by subtraction of the traces in Fig. 5*B* from those in Fig. 5*A*.

To obtain steady-state activation curves, conductance corresponding to peak currents was calculated $(G = I/(E - E_K)]$ and fitted to the Boltzmann equation,

$$G = G_{max}/\{1 + \exp[-(V_m - V_{1/2})/V_c]\},$$

where $G_{max}$ is the maximum conductance, $V_{1/2}$ is the half-activation voltage and $V_c$ is the slope. All three of these parameters were determined by the fit (we did not assume $G_{max}$). The steady-state voltage dependence for the anti-Kv2.1-sensitive current was well fitted by a single Boltzmann function, with half-activation ($V_{1/2}$) at $+3.8 \pm 1.1$ mV and slope $13.4 \pm 0.7$ mV. This was very similar to the whole current ($V_{1/2}$ $0.5 \pm 0.9$ mV, slope $14 \pm 0.7$ mV) and more depolarized than the remaining current ($V_{1/2}$ $-3 \pm 0.8$ mV, slope $14.2 \pm 0.7$ mV).

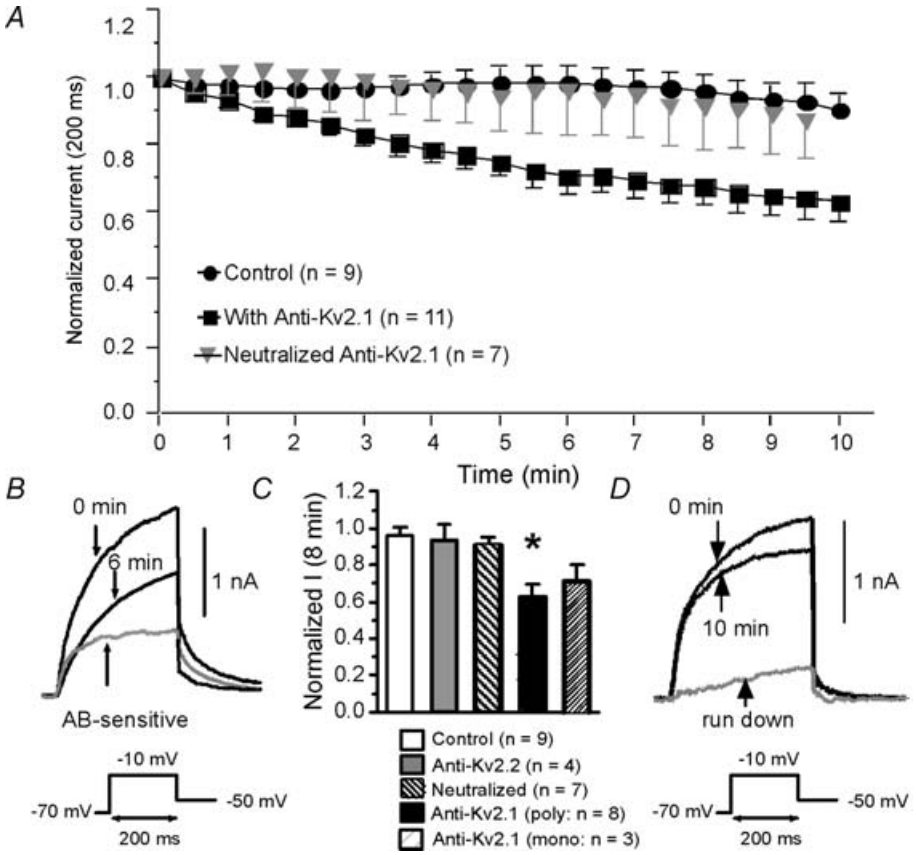


**Figure 4. Including anti-Kv2.1 in the pipette inhibited a slowly activating $K^+$ current**
*A*, currents were elicited by a voltage step to −10 mV from a holding potential of −70 mV. These steps were repeated every 10 s. The average current in the control (filled circles) and neutralized antibody (grey triangles) groups changed little over 8 min of recording (4% change). The decline in current was more rapid at times later than 8 min. In contrast, for the group with anti-Kv2.1 in the pipette, the initial decline was much steeper and the current was reduced by an average of 33% at 8 min (significantly different from control). *B*, a typical example of the effects of intracellular anti-Kv2.1 on the outward $K^+$ currents. During 6 min of intracellular diffusion, anti-Kv2.1 inhibited a persistent current (grey trace). The remaining current activated much more slowly than the anti-Kv2.1-sensitive current. *C*, histograms (mean ± S.E.M.) for four groups of pyramidal cells: control (without anti-Kv2.1: $n = 9$), anti-Kv2.1 neutralized by Kv2.1 antigen ($n = 7$), anti-Kv2.2 in the pipette ($n = 4$ cells), and anti-Kv2.1 in the pipette. Eight cells were recorded with the polyclonal anti-Kv2.1 and three cells with the monoclonal antibody. At 8 min, 38% of the outward $K^+$ current was reduced in the group with polyclonal anti-Kv2.1 and 30% with the monoclonal anti-Kv2.1 (combined: 33%). In the group with neutralized anti-Kv2.1 or with anti-Kv2.2, current reduction was only 8%. The control current declined by 4%. *Significant difference from control value ($P < 0.05$: ANOVA, Tukey's multiple comparison test). *D*, representative traces from a cell recorded with the control internal. Note the much slower activation of the subtracted, run-down current compared with anti-Kv2.1-sensitive current in *B*.

At −70 mV, a substantial fraction of the Kv2.1-mediated current was inactivated (see below). To determine whether the above data were biased to a subset of anti-Kv2.1-sensitive channels, we tested three cells (all P28) following a pre-pulse to −90 mV for 3 s to remove inactivation (Fig. 5*E–H*). The currents appear similar in form to those obtained from −70 mV and the activation voltage dependence of the anti-Kv2.1-sensitive current was very similar (compare Fig. 5*H* and 5*D*: after prepulses: $V_{1/2}$ 0.1 ± 1.7 mV, slope 13.2 ± 1.5 mV).

### Expression and properties of Stromatoxin-sensitive currents in the pyramidal cells

The Kv2.1 antibody sensitivity demonstates that Kv2.1 subunits are major contributors to the slowly inactivating current. It is likely that our data at 8 min diffusion time underestimate the contributions of Kv2.1 due to limits of accessibility of the antibody to the channels and complications due to due current run-down at later recording times (cf. Fig. 4). We therefore sought a complementary way to isolate Kv2 currents. rStromatoxin (ScTx) has been shown to be a potent blocker of both Kv2.1 and Kv2.2 ($K_d \approx 30$ nM in *Xenopus* oocytes: Escoubas *et al.* 2002). ScTX acts as a gating modifier, shifting activation to depolarized potentials. It also effectively blocks Kv4.2, a $K^+$ channel subunit responsible for one type of A current (Escoubas *et al.* 2002). We tested the effects of ScTx on $K^+$ currents in pyramidal neurons. $\alpha$-DTX and MTX were always used in the external solutions to exclude contributions of Kv1 channels to the recorded $K^+$ current.

To test for ScTx-sensitive currents, a 1 s test step to −10 mV from a holding potential of −70 mV was repeated every 10 s (Fig. 6*D*). ScTx (250–600 nM) caused a large, rapid and fully reversible reduction in the current for all tested pyramidal neurons (P15–P34: Fig. 6*A*). The block and wash out of persistent currents (measured at 200 ms) were each well fitted by a single exponential function. The time constants were 19 ± 3.8 s ($n = 16$) and 33 ± 5.8 s ($n = 12$) for onset of block and wash out, respectively

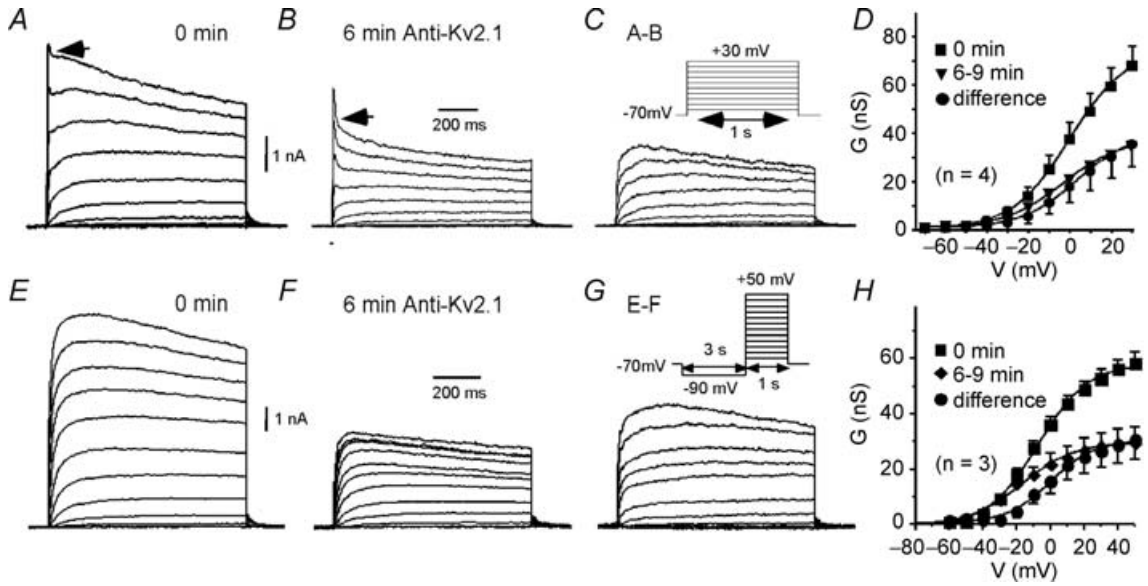


**Figure 5. Voltage-dependent activation of the anti-Kv2.1-sensitive current**
Outward $K^+$ currents were activated by series of depolarizing voltages in 10 mV increments from a holding potential of –70 mV (*A–D*) or –90 mV (*E–H*). *A*, example of currents recorded from one pyramidal cell just after break in to whole-cell mode (P20). Note the small fast, transient current (A-type: arrow). *B*, currents recorded at 6 min from the same cell. Because the slowly activating current was reduced, the A-type current was more obvious (arrow). *C*, subtraction of records in *B* from those in *A* reveals the antibody-sensitive current (inset: voltage protocol). *D*, steady-state activation curves for the non-A-type current components were obtained by fitting peak current amplitudes to the Boltzmann equation. The antibody (AB)-sensitive currents (●), obtained by subtracting the currents at 6–9 min from the currents at 0 min, had a half-activation potential of +3.8 mV with a slope of 13.4 mV. The remaining current (▼) activated at more negative potentials than the AB-sensitive current (half-activation at –3 mV, slope = 14.2 mV). *E*, representative traces for currents just after break-in from another cell (P28). In this cell, currents were elicited by steps to various potentials after a prepulse to –90 mV for 3 s (to remove inactivation, see inset in G). *F*, currents in the same cell after 6 min diffusion of polyclonal anti-Kv2.1. *G*, subtracted records (*E* − *F*) to indicate the AB-sensitive current (inset: voltage protocol). *H*, steady-state activation curve for averaged data from 3 cells using the protocol in *G*. The anti-Kv2.1-sensitive current had a $V_{1/2}$ of +0.1 mV (slope, 13.2 mV). The remaining current activated at more negative potentials ($V_{1/2}$, = −17 mV; slope, 15.7 mV).

(Fig. 6*B*). Under our recording conditions (100 $\mu$m $Cd^{2+}$), we noticed a developmental difference in our ability to detect a measurable A current in pyramidal cells. About 80% of cells at P20 or younger had measurable A current (8 of 10), compared with 22% of cells after P28 (8 of 36). The A current appears to be down regulated with age; however, the presence of $Cd^{2+}$ effectively blocks A current in many cells, so we did not study this in detail. In some cells (mostly from animals < P20), both the whole current ($\alpha$-DTX and MTX remaining) and the ScTx-sensitive current contained a small, fast activating, A-like component whose peak was at about 4 ms after step onset (Fig. 6*C*). This is consistent with ScTX block of Kv4 as well as Kv2 current. In pyramidal cells from other rats (mostly aged 4–5 weeks), the A-like component was not evident (Fig. 6*D*). At all ages, modest inactivation was observed in the ScTx-sensitive currents during a 1 s step.

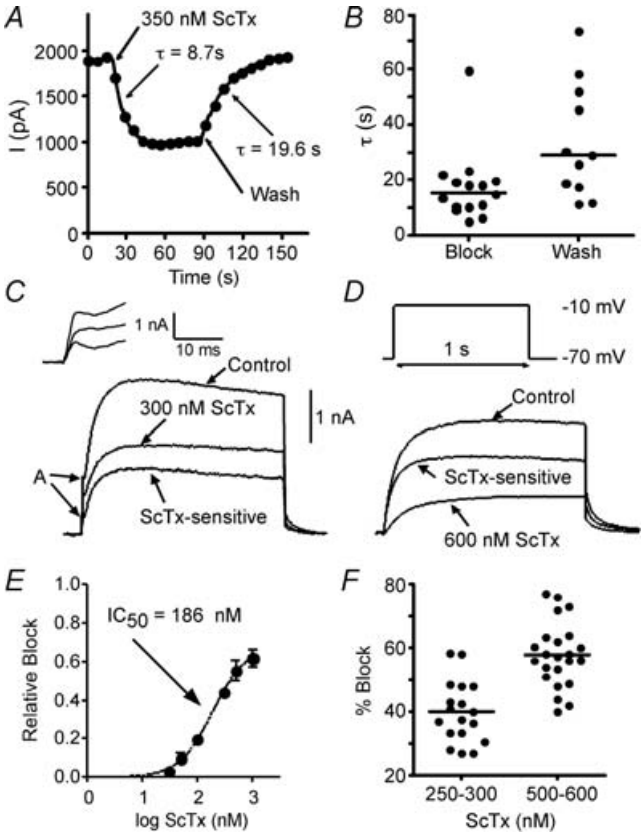


**Figure 6. rStromatoxin (ScTx), a $K^+$ channel blocker specific for Kv2 and Kv4 subunits, inhibited slowly inactivating $K^+$ current**
The voltage protocol used to obtain *A–F* is shown an inset in *D*. *A*, the effects of ScTx on $K^+$ current are reversible, allowing repetitive tests on the same cell. *B*, scatter plots for the time constants ($\tau$) for block of current and subsequent reversal (wash). For doses between 250 and 600 nM, the inhibition of outward current by ScTx can be described by an exponential function of time with a mean time constant of $19 \pm 4$ s. Reversal of the effects of ScTx occurred with a time constant of $33 \pm 6$ s. *C*, in pyramidal neurons from some rats (especially < 3 weeks: see text), a fast, A-like component was evident in the outward current ('A' and inset). In these cells, ScTx blocked both the transient component and a portion of the slowly inactivating current. *D*, for most mature pyramidal neurons (> 4 weeks: see text), this transient component was not prominent and no transient component is evident in the ScTx-sensitive current. Inset: voltage protocol. *E*, dose–response curve for ScTx. The relative block of the outward $K^+$ current by ScTx increases continuously with ScTx concentration. The effects by ScTx can be well fitted with a single Langmuir isotherm with an $IC_{50}$ of 186 nM. The data are plotted as mean ± S.E.M. *F*, the scatter plots show that percentage block of the outward $K^+$ current by ScTx was variable. Block by 500–600 nM ScTx varied from 41% to 79%, with a mean of 58 ± 2%. The mean values are indicated by horizontal lines.

**Table 1. Comparison of biophysical properties of anti-Kv2.1-sensitive and rStromatoxin-1 (ScTx)-sensitive currents**

| Activation | AB sensitive[1] | ScTx sensitive[2] |
|---|---|---|
| % block | 33 ± 5.7 (11) | 58 ± 2.1 (22) |
| $\tau$ at −10 mV (ms) | 75 ± 25 (4) | 69 ± 21 (4) |
| $V_{1/2}$ (mV) | 3.8 ± 1.1 (4) | −3.1 ± 0.8 (4) |
| Slope (mV) | 13 ± 0.7 (4) | 10.5 ± 0.6 (4) |
| Inactivation $\tau$ | | |
| at −10 mV (s) | 5.2 ± 1.5 (5) | 7.8 ± 2.1 (11) |
| $V_{1/2}$ (mV) | −62 ± 3.0 (6) | −60 ± 1.6 (7) |
| Slope (mV) | 11.5 ± 1.1 (6) | 12.5 ± 0.2 (5) |
| Recovery (at 100 mV) | | |
| ($\tau$ (ms)) | 793 ± 123 (9) | 980 ± 67 (8) |
| $E_{rev}$ (mV) | –- | −91.8 ± 2.4 (3) |

[1]AB, anti-Kv2.1, combined polyclonal ($n = 8$) and monoclonal ($n = 3$). [2]500–600 nM ScTx. Values are mean ± S.E.M.

The above results indicate that ScTx-sensitive currents consist of at least two distinct components. The first is A current, which is rapidly activating and inactivating. The second is a slowly activating and inactivating component which is Kv2 mediated. We concentrate here on the latter component and therefore restrict further analyses to cells which do not express measurable A current (generally P28–P35).

The dose–response relationship for the block by ScTx was tested in three cells (Fig. 6*E*). An $IC_{50}$ of 186 nM was obtained using the same fitting equation as for Fig. 3*B* and *D*. Two doses of ScTx higher than the $IC_{50}$ were tested in a large sample of the layer II/III pyramidal neurons (18 at 250–350 nM and 23 at 500–600 nM). The percentage block by 250–350 nM ScTx spanned 27% to 59% ($39.9 \pm 2.3$%; Fig. 6*F*, Table 1). For 500–600 nM ScTx, the percentage block covered a wide range between 40% and 80% ($57.7 \pm 2.1$%; Fig. 6*F*, Table 1). These data indicate that most of the slowly activating $K^+$ current in the pyramidal neurons was sensitive to ScTx. The wide range of percentage block suggests diversity of expression of the ScTx-sensitive current. There were no differences in percentage block by age of animal (data not shown).

### Do anti-Kv2.1 and ScTx block the same current component?

To test whether intracellular anti-Kv2.1 and ScTx block the same current component, we compared block by ScTx before and after action of 10 $\mu$g ml$^{-1}$ anti-Kv2.1. Whole cell recordings were obtained with internal solution containing anti-Kv2.1. Immediately after breaking into the cell, we recorded current amplitude and then tested block by 300 nM ScTx (Fig. 7). In five cells tested, the initial application of ScTx blocked 1122 ± 228 pA of current (50.8 ± 2.5%; Fig. 7*A* and *D*). We then allowed time for the Kv2.1 antibody to block channels. When we retested the response of the cells to ScTx after 8 and 12 min perfusion, the block by ScTx was greatly reduced to 510 ± 272 pA (34.4 ± 6.4%), indicating occlusion of the ScTx effect by anti-Kv2.1 (Fig. 7*A* and *D*). In these same five cells, anti-Kv2.1 blocked 789 ± 164 pA after 10–15 min (39 ± 14%). As a control, we tested a second application of ScTx after 8–12 min in three control cells. In these cells, the second application blocked as much current as the first application (Fig. 7*D*). For the cell in Fig. 7, we plotted the current sensitive to the first application of ScTx and the anti-Kv2.1-sensitive current (obtained by subtracting the current remaining at 15 min perfusion time from the initial current after break into whole-cell mode). The kinetics of the currents obtained by these two means were nearly identical (Fig. 7*C*). Collectively, these data suggest that anti-Kv2.1 and ScTx block the same current component. A further test is provided by comparison of the biophysical properties of anti-Kv2.1 and SCTx-sensitive currents (see below).

### Voltage dependence of ScTx effects

Previous studies in expression systems showed that inhibition of Kv2 currents by ScTx was voltage dependent, with reversal of apparent block at depolarized voltages (Escoubas *et al*. 2002). We examined this effect on the ScTx-sensitive currents in pyramidal neurons. Seven pyramidal neurons (P28–P30) were tested with a series of 200 ms voltage steps from a holding potential of −70 mV to various potentials in the control solution (containing $\alpha$-DTX and MTX) and after 600 nM ScTx (Fig. 8). A typical result for a cell without an A-type component is shown in Fig. 8*A*–*C*. ScTx (600 nM)-sensitive currents (Fig. 8*C*) activated more rapidly than the ScTx-insensitive currents (Fig. 8*B*). At more positive voltages (e.g. +30 mV trace), there was increased apparent inactivation of ScTx-sensitive currents. We hypothesized that this was due to voltage- and time-dependent reversal of the ScTx effect (cf. Escoubas *et al.* 2002).

Percentages of block ($100\% \times (I_{\text{whole}}/I_{\text{STX-sensitive}})/I_{\text{whole}}$) by 600 nM ScTx were calculated for each voltage step at two time points (20 and 200 ms) and summarized in Fig. 8*E*. The percentage block by ScTx at 20 ms was always larger than the percentage block at 200 ms. At more depolarized voltages (> 0 mV), the percentage block showed dependence on voltage. Block at 20 ms declined somewhat at potentials depolarized to 0 mV. The percentage block at 200 ms greatly decreased as voltage increased, however. These data probably reflect the kinetics of reversal of ScTX block at these depolarized potentials (Escoubas *et al.* 2002). Despite this voltage dependence,

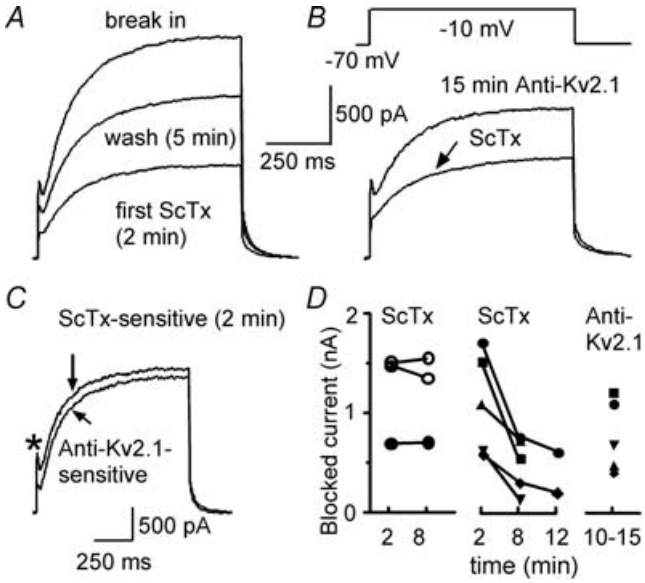


**Figure 7. Intracellular anti-Kv2.1 and ScTx both block the same Kv2.1-mediated current**
Currents were elicited by a 200 ms step to –10 mV from a holding potential of –70 mV (repeated every 10–30 s). Data were obtained from 5 cells with anti-Kv2.1 in the internal solution and three control cells without antibody. *A*, representative traces for a single cell for current just after break in to whole-cell mode, an initial application of 300 nM ScTx (2 min after break in) and subsequent wash out of ScTx (5 min after break in). Note the large block of current by ScTx and partial recovery. Recovery was not complete because continued perfusion of anti-Kv2.1 blocked current. *B*, traces from the same cell after 15 min of perfusion of anti-Kv2.1 and re-application of 300 nM ScTx. ScTx blocked less current after 15 min perfusion of anti-Kv2.1. *C*, subtracted records show the current blocked by the first application of ScTx (ScTx-sensitive) and current blocked by 15 min perfusion of anti-Kv2.1. The kinetics of the currents are strikingly similar, except that ScTx also blocked a fast transient current (*a small amount of transient current is also evident in the anti-Kv2.1 trace, probably due to run-down). *D*, summary data for ScTx effects in 3 control cells and 5 cells tested with anti-Kv2.1. Left, repeated application of 300 nM (○) or 600 nM ScTx (●) in control cells (no antibody) revealed little change in current blocked (left). Middle, in contrast, the amount of current blocked by ScTx was greatly reduced by perfusion with anti-Kv2.1 (at 8–12 min). Data from individual cells are indicated by the same symbol and a line between the points. Right, amount of current blocked by anti-Kv2.1 perfusion. There was a strong correlation between the amount of current blocked by anti-Kv2.1 perfusion and the amplitude of the decrease in ScTx block with time (Pearson $r = 0.9874$). The effects of ScTx and anti-Kv2.1 for the same cells are indicated by the same symbols.

ScTx is a useful tool for testing the expression and functions of Kv2 channels. The ScTx effects are specific and rapid (thus less interference from run-down artifacts). To minimize the voltage-dependent unblock, we used test steps to −10 mV for all subsequent experiments.

### Voltage dependence of steady-state activation

In four cells where no A-like component was seen (P28–P30), conductance was calculated from peak currents and fitted with the Boltzmann equation (see above). The half-activation potential of the ScTx-sensitive current was $-3.1 \pm 0.8$ mV and the slope was $10.5 \pm 0.6$ mV ($n = 4$: Fig. 8*F*). This value is probably biased in the hyperpolarized direction, due to reversal of ScTX block at depolarized potentials. The whole current had a half-activation voltage of $1.7 \pm 1$ mV and slope $12.2 \pm 0.6$ mV.

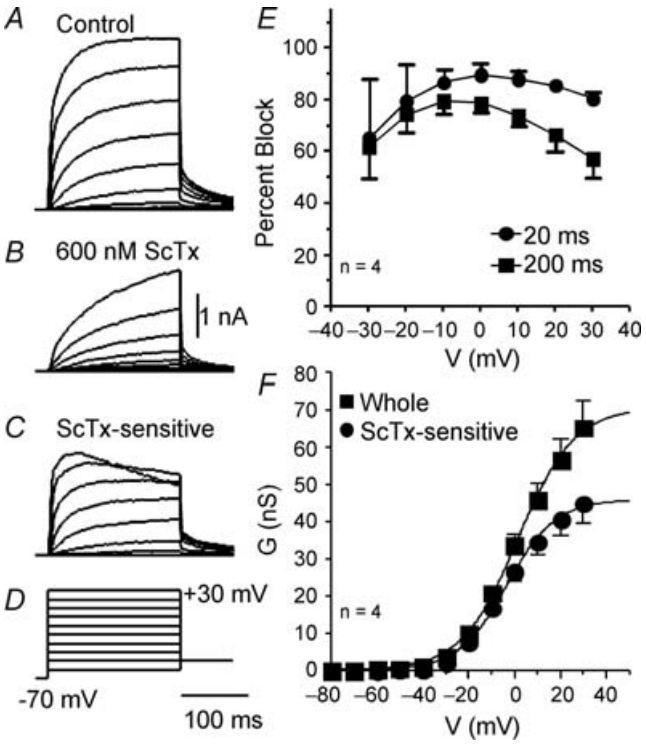


**Figure 8. Voltage-dependent inhibition by ScTx and activation of ScTx-sensitive current**
Currents were elicited by a series of voltage steps from −60 mV to +30 mV, repeated at 10 s intervals. The holding potential was −70 mV. *A*, a typical example of currents recorded in the control solution (P28). *B*, currents recorded from the same cell after application of 600 nM ScTx. The ScTx-insensitive currents activate more slowly than the ScTx-sensitive current. *C*, ScTx-sensitive current was obtained by subtraction of traces in *B* from those in *A*. Note the similarity in kinetics to the anti-Kv2.1-sensitive current in Fig. 4*B*. One exception is that the ScTx-sensitive current elicited by the step to +30 mV showed a rapid decline in amplitude during the step. This finding is consistent with known, voltage-dependent effects of ScTx. *D*, voltage protocol for *A*–*C*. *E*, voltage dependence of ScTx effects. Percentage block at 20 ms and 200 ms for voltage steps to several potentials. At potentials depolarized to −10 mV, the percentage block at 20 ms is reduced. This is more dramatic at 200 ms into the step than at 20 ms, reflecting the kinetics of the voltage-dependent reversal of the ScTx effect. *F*, steady-state activation curve for the slowly activating, ScTx-sensitive currents. Peak *G* is plotted for averaged data from 4 cells without a detectable A current (mean ± S.E.M.). The half-activation potential for the ScTx-sensitive current was −3 mV (slope, 10.5 mV).

### Reversal potential

To further determine the specific properties of slowly activating ScTx-sensitive currents, tail currents were recorded with and without 600 nM ScTX (Fig. 9). Voltage was stepped to −10 mV for 200 ms from a holding potential of −70 mV, then stepped down to different potentials (−110 to −40 mV). Six cells (P20–38) were recorded from that did not show prominent A currents. Figure 9*A* shows recordings of the ScTx-sensitive current from a typical pyramidal neuron (P20). Tails of ScTx-sensitive currents demonstrated a reversal potential at $-91.8 \pm 2.4$ mV (Fig. 9*B*), which agrees well with the calculated $E_k$ (−96.8 mV for internal $K^+$ of 140 mM and external $K^+$ of 3 mM: determined by the Nernst equation). Two cells were also tested in high $K^+$ (50 mM) solution. Again, the tested reversal potential for the ScTx-sensitive currents approximated the calculated $E_k$ (−27.0 mV *versus* −25.9 mV: Fig. 9*B*). The tails of the ScTx-insensitive current reversed polarity at $-83.5 \pm 2.0$ mV in 3 mM extracellular $K^+$ and also showed a Nernstian shift with raised extracellular $K^+$ (Fig. 9*B*). These data indicated that the channels that underlie the ScTx-sensitive and -insensitive currents are very $K^+$ selective.

### Activation and deactivation kinetics

To characterize the kinetics of the slowly inactivating component, currents were recorded at a step potential of −10 mV from a holding potential of −70 mV. The activation time constant was obtained by fitting the currents to the following equation:

$$I = I_o[1 - \exp(t/\tau)]^m,$$

where $I$ is current, $I_o$ is the initial current, $t$ is time, $\tau$ is the time constant, and $m$ is the activation coefficient. The best $m$ value was between 1 and 1.3. For comparisons, $m$ was set to be 1 for all currents. We only used cells with no visible A current and we fitted data from 0 to 200 ms. We used a single first order exponential function to fit the deactivation tails.

Activation and deactivation time constants for the slowly activating components in both ScTx-sensitive and ScTx-insensitive currents are shown in Fig. 9*C*. Eighteen pyramidal neurons were tested in ScTx (P20–P38: 250–600 nM). The activation time constants of the ScTx-sensitive currents showed no dependence on the

concentration of ScTx (data not shown), indicating the high specificity of ScTx to the targeted channels. The mean activation time constant for ScTx-sensitive current at −10 mV was 69 ± 42 ms (Table 1).

The ScTx-sensitive component was faster than the remaining component for voltages above −30 mV. We also tested the activation time constants for the anti-Kv2.1-sensitive current ($n = 4$ cells). They were very similar over the whole voltage range to those obtained for the ScTx-sensitive component (e.g. 74 ± 25 ms at −10 mV; Table 1, Fig. 9*D*), consistent with the same channels being targeted by both anti-Kv2.1 and ScTx.

### Inactivation and recovery

Inactivation kinetics of the 600 nM ScTx-sensitive component were examined in 15 cells (P17–30). Voltage was held at −70 mV and stepped to −10 mV for 1–3 s. Figure 10*A* shows a typical example for currents in control solution as well as the currents sensitive and insensitive to 600 nM ScTx. In 11 of 15 cells, the ScTx-sensitive currents reached a peak between 140 ms and 380 ms after the step (Fig. 10*A*) and then the currents slowly decayed. The inactivation process was well fitted by an exponential function, with time constants between 2.0 s to 25.5 s (7.8 ± 2.1 s: Fig. 10*B*). The other four cells and all currents remaining after ScTx did not inactivate over 3 s. We obtained 1 s steps to −10 mV for the anti-Kv2.1-sensitive current in six cells (all P32). One cell did not inactivate over 1 s. For the other five cells, the inactivation time constant was 5.2 ± 1.5 s.

Holding potential sensitivity of the 600 nM ScTx-sensitive component was tested in three cells (all P30). Voltage was held at −70 mV, and then stepped to −40 mV for variable lengths of time (0–7 s). The inactivation prepulse was followed by a 200 ms test step to −10 mV. As shown in Fig. 10*C* and 80% of the ScTx-sensitive current was inactivated at −40 mV with a time constant of 2.5 ± 0.3 s. The ScTx-insensitive current showed no inactivation within 7 s at −40 mV. In another group of five cells (data not shown), currents were first recorded in control and 600 nM ScTx solutions at a holding potential of −40 mV. The holding potential was then decreased to −80 mV. Three minutes were allowed to elapse at both holding potentials before recording. The amplitude of the ScTx-sensitive current again demonstrated greater holding potential dependence than the ScTx-insensitive current. Collectively, these data show that the ScTx-sensitive current inactivates at potentials below the activation range (cf. Klemic *et al.* 1998). This confers great holding potential sensitivity on the current.

The steady-state voltage dependence of inactivation of the ScTx-sensitive current was studied in seven cells (P28–P30). Voltage was held at −70 mV and stepped to various inactivation potentials for 5 s. These prepulses were followed by a 400 ms test pulse to −10 mV. Figure 10*D* shows a typical example of the 600 nM ScTx-sensitive currents after 5 s inactivation at various potentials. Peak currents were measured during the −10 mV test pulse and were fitted by the Boltzmann equation of the form:

$$I/I_{\max} = 1/\{1 + \exp[(V - V_{1/2})/V_c]\}$$

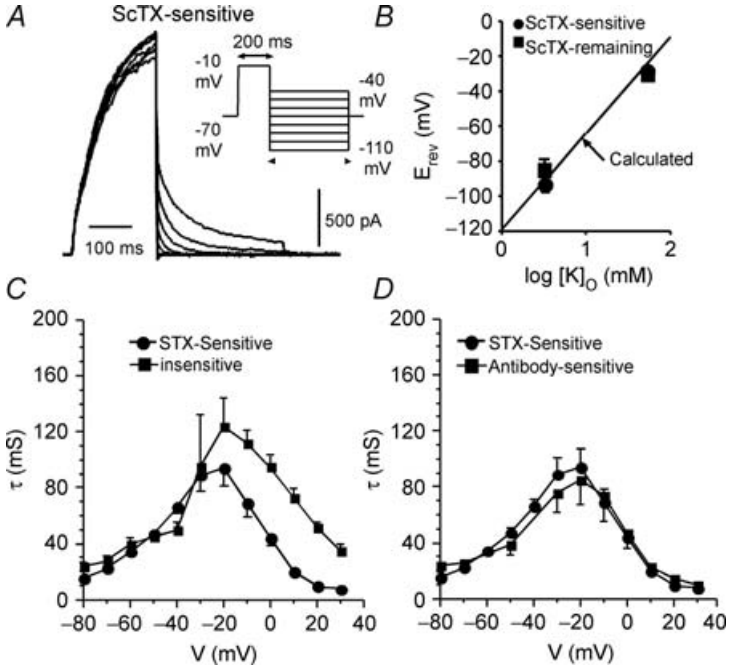


**Figure 9. Reversal potenial and activation and deactivation kinetics of the $K^+$ currents sensitive to polyclonal anti-Kv2.1 or ScTx (600 nM)**
Time constants were obtained by fitting currents with a single exponential function. *A*, an example of tail currents sensitive to 600 nM ScTx (P20). The tail currents were elicited by a series of different voltages stepped down from a 200 ms activating potential step of –10 mV (inset). *B*, both the ScTx-sensitive and –insensitive current components reversed polarity near $E_K$ (3 mM $K^+$). The reversal potential also shifted in a Nernstian manner with elevated extracellular $K^+$ (50 mM $K^+$). These data indicate that the channels underlying the ScTx-sensitive and –insensitive currents are very potassium selective. *C*, activation and deactivation time constants for the ScTx-sensitive and ScTx-insensitive currents. ScTx-sensitive and –insensitive currents have similar kinetics at negative potentials, with the ScTx-insensitive currents being slower at potentials depolarized to ∼−20 mV. *D*, the activation and deactivation time constants of the ScTx-sensitive and the anti-Kv2.1-sensitive currents were very similar over the entire voltage range tested.

(Fig. 10*E*). The ScTx-sensitive currents had a half-inactivation potential of $-60.1 \pm 1.6$ mV and the slope was $12.5 \pm 0.2$ mV (Fig. 10*E* and *F*). About 30% of the ScTx-insensitive current inactivated, with a half-inactivation potential of $-83.6 \pm 2.5$ mV (slope $11.0 \pm 1.6$ mV: Fig. 10*E*). The whole current had a half-inactivation potential of $-62 \pm 2.0$ mV and the slope was $14 \pm 0.5$ mV ($P < 0.001$; $n = 7$).

In six cells, steady-state inactivation was obtained for the current blocked by intracellular anti-Kv2.1. The half-inactivation voltages ($-62 \pm 3.0$ mV) and slopes ($11.5 \pm 1.1$ mV) for these cells were very similar to values obtained with ScTx (Table 1; Fig. 10*E* and *F*).

Recovery from inactivation for ScTx-sensitive current was tested in eight cells (P28–30) using the voltage protocol shown in the lower portion of Fig. 11*A*. Currents were first inactivated by holding at $-48$ mV for at least 12 s. Then, a 200 ms test pulse to $-10$ mV was delivered and followed by a recovery pulse at $-100$ mV of various durations. At the end of the recovery pulses, the test pulse was delivered

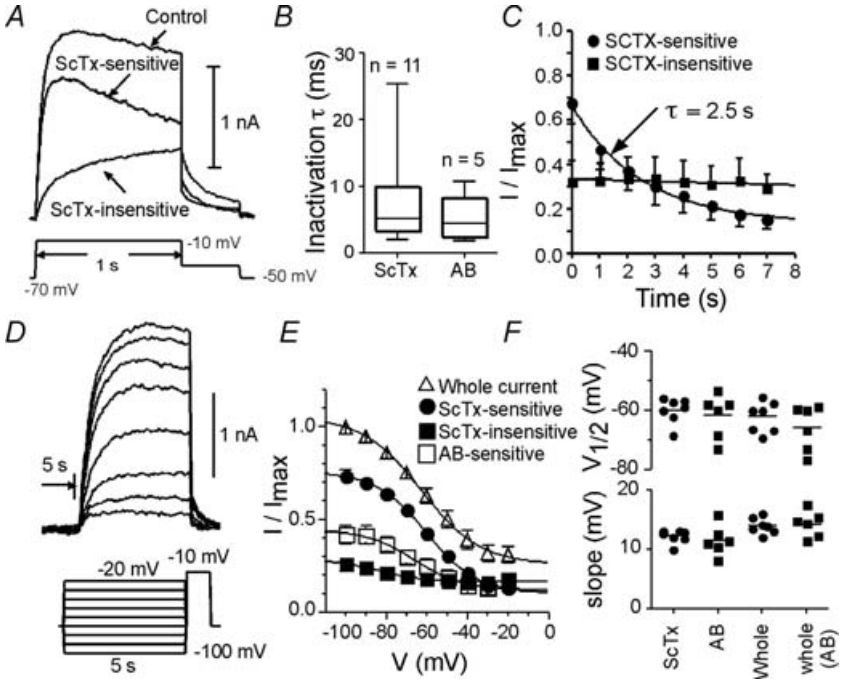


**Figure 10. Inactivation of ScTx-sensitive currents**
*A*, current traces elicited by 1–3 s voltage steps to $-10$ mV from a holding potential of $-70$ mV (protocol below traces). Shown are a control trace and currents sensitive and insensitive to 600 nM ScTx (note difference in kinetics between ScTx-sensitive and -insensitive currents) (P30). *B*, box plot summarizing the time constant ($\tau$) for inactivation determined by fitting the current decline (at $-10$ mV) with an exponential function. The inactivation time constants for the ScTx-sensitive current were between 2 and 26 s, with a median at 5.2 s ($n = 11$ cells). For the AB-sensitive current, median $\tau$ was 4.5 s ($n = 5$ cells). *C*, holding potential sensitivity of ScTx-sensitive and -insensitive currents. Currents were elicited by a step from $-70$ to $-10$ mV (200 ms; not shown). The stimulus was repeated at 10 s intervals. Holding potential was then changed to $-40$ mV. The plots show the amplitude of currents elicited by the test stimulus as a function of time after the holding potential change. The peak amplitude of the ScTx-sensitive currents decreased with time at $-40$ mV. The changes were well fitted by an exponential function, with a time constant of $2.5 \pm 0.3$ s. The ScTx-sensitive currents elicited from the $-40$ mV holding potential were much smaller than the currents recorded from $-80$ mV holding potential. This strong holding potential dependence of the ScTx-sensitive current is similar to the TEA-sensitive currents (Fig. 3). *D*, representative traces for steady-state inactivation of ScTx-sensitive current after 5 s inactivation at various potentials from $-100$ mV to $-20$ mV (P30). Voltage protocol is shown as inset below. A series of 5 s inactivation voltage steps of varied potentials were delivered from a holding potential of $-70$ mV every 15 s and closely followed by a 400 ms test voltage step to $-10$ mV. *E*, steady-state inactivation curves were obtained by fitting the averaged recordings from 10 cells with the Boltzmann equation. The ScTx-sensitive currents (●) had a half-inactivation potential of $-60$ mV (slope, 12.5 mV). Average data from 6 cells where steady-state inactivation was tested for the polyclonal anti-Kv2.1-sensitive current are illustrated by open squares (P30; $V_{1/2} = -62$ mV, slope = 11.5 mV). The data are very similar to the ScTx-sensitive currents. Most of the ScTx-insensitive current (■) did not inactivate with this protocol. The half-inactivation potential for the ScTx-insensitive component that did inactivate was $-87$ mV. *F*, scatter plots summarizing the half-inactivation and slope data for ScTx-sensitive and anti-Kv2.1 (AB)-sensitive current. The data are very similar for the two ways of isolating Kv2.1 currents.

again. Figure 11*A* shows typical ScTx-sensitive currents. Most ScTx-sensitive currents had been inactivated at −48 mV. Their recovery process at −100 mV could be well characterized by a single exponential function of time with a time constant of 918 ± 67 ms ($n = 8$). The remaining currents had two components, one was not inactivated at −48 mV, and one that recovered with a time constant of 170 ± 7 ms ($n = 8$). We tested recovery from inactivation in nine cells (P28–P32) recorded in the presence of the polyclonal anti-Kv2.1 antibody. At −100 mV, the recovery time constant was not significantly different from the ScTx-sensitive current in these cells (793 ± 123 ms: data not shown).

## Discussion

To fully understand the function of voltage-activated potassium channels in native membranes requires knowledge of $K^+$ channel abundance, distribution and activity in native excitable membranes. Of particular interest is the molecular basis for the slowly inactivating $K^+$ currents. Overlapping biophysical properties and sensitivities to 4-AP and TEA make it difficult to link currents identified by those means with specific channel subunits. In addition, phosphorylation state (Misonou *et al.* 2004) and auxiliary channel subunits (Salinas *et al.* 1997; Kerschensteiner & Stocker, 1999) can alter biophysics and pharmacology (Richardson & Kaczmarek, 2000).

We report here that Kv2.1 subunits are the major contributor to the slowly inactivating $K^+$ current in neocortical pyramidal neurons. We found expression of both Kv2.1 and Kv2.2 mRNAs and proteins in pyramidal cells, with a pronounced difference in the localization of the two subunits. Whereas Kv2.1 subunits were expressed by virtually all pyramidal cells in the soma and proximal apical dendrite, Kv2.2 subunit protein was primarily expressed throughout the apical dendrites of a subset of pyramidal cells from deep layers (V/VI). We identified Kv2-mediated currents with intracellular application of a Kv2.1 antibody and compared the anti-Kv2.1-sensitive currents with current sensitive to the gating modifier rStromatoxin-1 (ScTx). A striking finding was that the Kv2.1 current was very holding potential sensitive.

Our finding of current blocked by anti-Kv2.1 (but not neutralized anti-Kv2.1 or anti-Kv2.2) is strong evidence for involvement of Kv2.1 subunits underlying the slowly inactivating current. Most of our experiments employed the polyclonal anti-Kv2.1 (Trimmer, 1991) previously shown to block Kv2.1 currents in cultured hippocampal pyramidal neurons (Murakoshi & Trimmer, 1999) and smooth muscle (Archer *et al.* 1998; Lu *et al.* 2002). We obtained similar results with a monoclonal antibody to the C-terminus of Kv2.1 (NeuroMab).

### Expression of Kv2.1 and Kv2.2 subunits

Kv2.1 subunits are widely expressed in the mammalian brain (Frech *et al.* 1989; Hwang *et al.* 1993; Du *et al.* 1998; Trimmer & Rhodes, 2004; Misonou *et al.* 2005). In hippocampal and layer V neocortical pyramidal cells (Hwang *et al.* 1993; Du *et al.* 1998; Antonucci *et al.* 2001) and in spinal motoneurons (Muennich & Fyffe, 2004), Kv2.1 subunits are localized to variably sized clusters on soma and proximal dendrites. These subunits are not found in axons. The clustering is dependent upon phosphorylation state; dephosphorylation causes dispersion of the clusters

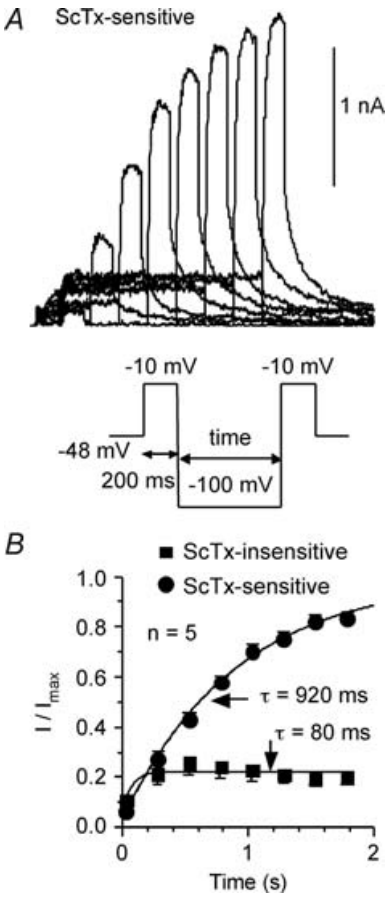


**Figure 11. Recovery from inactivation of the ScTx-sensitive currents was tested in 5 cells using a protocol shown in the lower part of *A***

The currents were inactivated at a holding potential of −48 mV. A 200 ms test pulse of −10 mV was delivered and followed by a recovery voltage step of −100 mV. The duration of the recovery voltage step varied from 0.02 to 1.77 s with increments of 0.25 s. A second test pulse of −10 mV was delivered after the recovery voltage step. Currents in response to the second test pulse were analysed relative to the first test step. *A*, typical example of the recovered ScTx-sensitive currents (P30). *B*, the peak recovered ScTx-sensitive currents can be well fitted by an exponential function, yielding a recovery time constant of 920 ms. Similar data were obtained for the AB-sensitive current (see text). The recovery time constant for the ScTx-insensitive component was 170 ms.

(Misonou *et al.* 2004). In the present study, we confirmed this localization of Kv2.1 subunits to clusters in soma and proximal dendrites of pyramidal cells. Virtually all pyramidal cells expressed Kv2.1 mRNA and protein.

Kv2.2 subunits are not as widely expressed as Kv2.1. In cortex, they have been reported to primarily localize to interneurons (Hwang *et al.* 1993). We found that a large percentage of pyramidal cells in all layers also expressed Kv2.2 mRNA. We also found striking differences in the expression of Kv2.1 *versus* Kv2.2 protein in neocortical pyramidal neurons. In contrast to the soma/proximal dendritic expression of Kv2.1 in all pyramidal cells, Kv2.2 subunits were not clustered in the manner of Kv2.1 subunits and were primarily localized to apical dendrites of a subset of deep (layers V/VI) pyramidal cells. These differences in distribution are consistent with the idea that Kv2.1 and Kv2.2 subunits are not combined in heteromultimeric channels *in situ* (Blaine & Ribera, 1998, 2001; Lim *et al.* 2000).

The ultrastructural findings for Kv2.2 were intriguing in that the bulk of the staining looked vesicular and these vesicles were distributed throughout the dendrites, suggestive of transport of the vesicles through the apical dendrites. Perhaps despite limited expression in the plasma membrane, these subunits are subject to rapid turnover.

### Kv2.1 subunits contribute to slowly inactivating current

Due to their nearly ubiquitous distribution, Kv2.1 subunits are often assumed to underlie the dominant delayed rectifier current, although this has only been shown in a small number of neuron types. Murakoshi & Trimmer (1999) used intracellular application of a polyclonal antibody to the C-terminus of the Kv2.1 subunit to identify Kv2.1 as the major contributor to the delayed rectifier current in cultured hippocampal pyramidal neurons. This was later confirmed by antisense treatment in organotypic slice cultures of hippocampus by Du *et al.* (2000). Genetic alterations of expression have also implicated Kv2.1 subunits as underlying the delayed rectifier in heart and sympathetic ganglia (Xu *et al.* 1999; Malin & Nerbonne, 2002) and cultured neocortical neurons (Pal *et al.* 2003). Intracellular Kv2.1 antibodies have implicated Kv2.1 in the delayed rectifier of smooth muscle cells (Archer *et al.* 1998; Lu *et al.* 2002). Kv2.2 subunits have been linked to delayed rectifier currents in *Xenopus* spinal neurons (Blaine & Ribera, 1998, 2001).

We used intracellular application of the polyclonal Kv2.1 antibody originally developed by Trimmer (1991) to demonstrate that Kv2.1 subunits were the dominant contributor to the slowly inactivating $K^+$ current in layer II/III pyramidal cells of rat neocortex. We obtained similar results with a monoclonal antibody to an overlapping C-terminal sequence. Current block by the antibody definitively identified Kv2.1 channels as a major contributor to the slowly inactivating $K^+$ current. These data are consistent with a study on cultured neurons from visual cortex, where a dominant-negative strategy indicated that most of the current was mediated by Kv2.1 channels (Pal *et al.* 2003). The antibody blocked 25–50% of the non-Kv1 current in our study (at 6–8 min). This is probably an underestimate of the Kv2.1 contribution due to limitations of accessibility of the antibody to the channels and complications with run-down at times longer than ~8 min perfusion. Currents from cells without antibody or with neutralized antibodies were stable over this time period (4–8% reduction in current) and the current which runs down has very slow activation kinetics, compared with the anti-Kv2.1-sensitive current (Fig. 4).

The affinity of the slowly inactivating current to TEA was also consistent with Kv2.1 channels, but TEA is a notoriously non-selective channel blocker. Because of these limitations, we sought another means to identify Kv2 channel contributions. We used the peptide ScTx, a selective Kv2 (and Kv4) gating modifier that shifts activation to much more depolarized potentials (Escoubas *et al.* 2002). A subset of the pyramidal cells expressed an obvious A-type current. In those cells, in addition to blocking a slowly inactivating current, ScTx blocked the A-type current, consistent with block of Kv4 channels that underlie this current (Yuan *et al.* 2005). To isolate effects on slowly inactivating current, we selected for cells which did not express substantial transient current (Kv4.2-mediated: Yuan *et al.* 2005) to isolate Kv2.1 currents for characterization. In those cells, ScTx caused a reversible apparent block of slowly inactivating current in a dose-dependent manner. We found that 600 nM ScTx blocked ~60% of the slowly inactivating current (at −10 mV). The apparent block by ScTx was clearly voltage dependent, with reversal at voltages positive to 0 mV. Thus, ScTx may also underestimate Kv2 contribution to the slowly inactivating current.

We demonstrated occlusion of ScTx effects by the Kv2.1 antibody. We also showed that the ScTx-sensitive current and current blocked by anti-Kv2.1 had very similar kinetics and voltage dependence of both activation and inactivation. Recovery from inactivation was also similar. No statistical differences were found for any of these measurements between ScTx- and anti-Kv2.1-sensitive currents (Table 1). These data suggest that anti-Kv2.1 and ScTx both block the same current mediated by Kv2.1 subunits. Considering our findings that Kv2.2 subunits were primarily expressed in apical dendrites of a subset of layer V/VI pyramidal cells and our recordings were restricted to truncated pyramidal cells from supragranular layers (II/III), it is likely that the ScTx-sensitive current was almost exclusively due to Kv2.1 channels.

### Biophysical properties of Kv2.1 currents in layers II/III pyramidal cells

We found that ScTx-sensitive and Kv2.1 antibody-sensitive currents were very similar in terms of the kinetics and voltage dependence of activation (all voltages) and inactivation. Activation began at similar voltages. The ScTx-sensitive current had a slightly more negative steady-state activation voltage, perhaps due to voltage-dependent reversal of the ScTx effect at more depolarized potentials. Anti-Kv2.1- and ScTx-sensitive currents also inactivated at similar rates and at similar voltages (Table 1) and recovered from inactivation at similar rates. These data strengthen our conclusion that ScTx blocks the same population of Kv2.1 channels as the Kv2.1 antibody. When using ScTx, we restricted test potentials to −10 mV or less depolarized to minimize the voltage-dependent reversal of ScTx effects.

Both the anti-Kv2.1- and the ScTx-sensitive current began to activate depolarized to ∼−40 mV and the half-activation voltage was consistently more depolarized than the remaining current. The half-activation voltage was also more depolarized than we previously found for the $\alpha$-DTX-sensitive component (Guan *et al.* 2006). The ScTx-sensitive current reversed very close to $E_K$, suggesting high $K^+$ selectivity of the underlying channels.

At −10 mV, the time constant for inactivation of the ScTx-sensitive current was slow ($\tau \approx 7$ s). Similar data were obtained with anti-Kv2.1. Steady-state half-inactivation voltage was ∼−60 mV for both the anti-Kv2.1- and ScTx-sensitive currents. We found the ScTx-sensitive current to be very holding potential sensitive. At −40 mV, most of the current inactivated with a time constant of 2.5 s. This is consistent with inactivation from an intermediate closed state, a property of Kv2.1 channels in some systems (Klemic *et al.* 1998). Recovery from inactivation had a time constant of ∼1 s at −100 mV.

For the most part, these findings were consistent with Kv2.1-derived currents in other neurons (Klemic *et al.* 1998; Thorneloe & Nelson, 2003) or expression systems (Shi *et al.* 1994; Murakoshi *et al.* 1997; Kerschensteiner & Stocker, 1999). Kv2 channels are generally considered to be slowly activating, slowly inactivating currents that require relatively depolarized membrane potentials for activation (cf. Storm, 1990; Misonou *et al.* 2005). The electrophysiological properties of Kv2.1 are somewhat different in different cell backgrounds, however (Mohapatra & Trimmer, 2006). It is unclear how much of the biophysical diversity is due to cell background and how much is due to the different preparations and protocols which have been employed across laboratories. For example, dissociated neurons allow excellent spatial voltage control but the cells have been subjected to enzymatic treatment. Cultured neurons and neurons in acute slices may have extensive processes that create problems with space clamp.

In expression systems, half-activation varies between −3 mV to +12 mV (Shi *et al.* 1994; Murakoshi *et al.* 1997; Salinas *et al.* 1997; Kramer *et al.* 1998). Shi *et al.* (1994) reported half-activation at +11 mV in Cos-1 cells. Murakoshi *et al.* (1997) obtained a value of −3 mV in the same Cos-1 cells. In *Xenopus* oocytes, values vary from +1 to ∼+20 mV (Kerschensteiner & Stocker, 1999; Richardson & Kaczmarek, 2000). These values are hyperpolarized compared with cultured hippocampal pyramidal cells (+17 mV: Mohapatra & Trimmer, 2006; +15 mV: Murakoshi & Trimmer, 1999). Our findings are consistent with this range. Our data for activation voltage dependence agree well with Kv2.1-mediated currents in acutely isolated bullfrog ganglia (+3 mV: Klemic *et al.* 1998) or smooth muscle (1.1 mV: Thorneloe & Nelson, 2003). Our data are also consistent with values for $I_K$ (defined by TEA sensitivity and biophysics) in acute slices and dissociated neocortical (−7.6 to +3.6 mV: Foehring & Surmeier, 1993; Zhou & Hablitz, 1996; Locke & Nerbonne, 1997; Korngreen & Sakmann, 2000; Bekkers, 2000*b*) and hippocampal (Klee *et al.* 1995) pyramidal cells. These data are consistent with $I_K$ being largely due to Kv2 channels.

In expression systems, Kv2.1 channels are relatively insensitive to holding potential (Shi *et al.* 1994; Salinas *et al.* 1997; Kramer *et al.* 1998; Kerschensteiner & Stocker, 1999; Murakoshi & Trimmer, 1999; Mohapatra & Trimmer, 2006). The half-inactivation potential in COS-1 cells was −25 mV (Shi *et al.* 1994) and between −35 and −20 mV in oocytes (Kerschensteiner & Stocker, 1999; Richardson & Kaczmarek, 2000). In cultured hippocampal pyramidal cells, the reported value was −26 mV (Mohapatra & Trimmer, 2006). In contrast, we found that Kv2.1-mediated currents in layer II/III pyramidal cells inactivated > 80% at −40 mV. We found the steady-state half-inactivation voltage to be ∼−60 mV in neocortical layer II/III pyramidal cells. This is similar to isolated urinary bladder smooth muscle (−61 mV: Thorneloe & Nelson, 2003). These data are in general agreement with steady-state inactivation of the TEA-sensitive, slowly inactivating $I_K$ in pyramidal neurons (−54 to −67 mV: patches from acute slice: Bekkers, 2000*b*; Korngreen & Sakmann, 2000; acutely dissociated: Foehring & Surmeier, 1993; Klee *et al.* 1995; Locke & Nerbonne, 1997). Again, these data are consistent with $I_K$ being largely due to Kv2 channels.

Our findings for activation and inactivation kinetics are similar to Kv2.1 currents in expression systems. These kinetics are also similar to those of $I_K$ in neocortical pyramidal cells (patches from acute slices: Bekkers, 2000*b*; Korngreen & Sakmann, 2000; acutely dissociated: Foehring & Surmeier, 1993; Locke & Nerbonne, 1997). We found recovery from inactivation occurred with time constants of ∼1 s in layer II/III cells. This is similar to Kv2.1 in *Xenopus* oocytes (Kerschensteiner & Stocker,

1999) and $I_K$ in layer V cells (Bekkers, 2000*a*,*b*) or unidentified acutely dissociated pyramidal cells from all layers (Foehring & Surmeier, 1993). Somewhat faster recovery was reported for $I_K$ in acutely dissociated callosal projecting pyramidal cells (~79 ms: Locke & Nerbonne, 1997).

Kv2.1 can form heteromultimeric channels with almost all silent Kv $\alpha$ subunits (e.g. Kv5, 6, 8, 9: Castellano *et al.* 1997; Kramer *et al.* 1998). Coexpression of Kv2.1 with these auxiliary subunits alters expression and modifies the biophysical properties of Kv2.1 currents. Interestingly, the hyperpolarized inactivation and activation of native Kv2.1-mediated currents in layer II/III pyramidal cells are very similar to Kv2.1 coexpressed with Kv5 (Kramer *et al.* 1998), Kv6 (Kramer *et al.* 1998) or Kv9 subunits (Salinas *et al.* 1997; Richardson & Kaczmarek, 2000). This suggests the intriguing possibility that the properties of currents in layer II/III pyramidal cells are due to coexpression of Kv2.1 plus silent auxiliary subunits. This has also been suggested for urinary bladder smooth muscle (Thorneloe & Nelson, 2003). These silent subunits are expressed in cortex (Salinas *et al.* 1997). Another possibility is that phosphorylation state varies between acutely dissociated layer II/III pyramidal cells and cultured hippocampal pyramidal neurons (Misonou *et al.* 2004) or expression systems. Dephosphorylation shifts activation and inactivation to more hyperpolarized potentials in cultured hippocampal pyramidal neurons (Misonou *et al.* 2004).

### Predictions for function

Based upon its dominant contribution to the outward current and localization of channels, Kv2.1 subunits would be expected to have important roles in regulating excitability of the soma/proximal apical dendritic compartment (Larkum *et al.* 1999) of neocortical pyramidal neurons. The localization of Kv2.2 subunits suggests a more restricted role in regulating distal dendritic excitability.

Because of relatively slow kinetics and positive activation range, we predict that Kv2.1 channels should play minimal roles in regulating subthreshold excitability but should be a major contributor to regulating repetitive activity in layer II/III pyramidal cells. The high holding potential sensitivity suggests that available Kv2.1 current will be highly subject to cell membrane potential and activation history. In particular, Kv2.1 contributions would be greater when the cell is initially in the 'down state' observed during slow oscillations during slow wave sleep or anaesthesia (Stern *et al.* 1997). The Kv2.1 brake on excitability would tend to reinforce this down state. Kv2.1 channels would be much less available during the 'up state' of the slow oscillations or in awake behaving animals (Stern *et al.* 1997). Again, less $K^+$ conductance would facilitate activity during this state. All of these functions are probably subject to modulation by transmitters and pyramidal cell activity (Misonou *et al.* 2004, 2005).

## References


Antonucci DE, Lim ST, Vassanelli S & Trimmer JS (2001). Dynamic localization and clustering of dendritic Kv2.1 voltage-dependent potassium channels in developing hippocampal neurons. *Neuroscience* **108**, 69–81.

Archer SL, Souil E, Dinh-Xuan AT, Schremmer B, Mercier JC, El Yaagoubi A, Nguyen-Huu L, Reeve HL & Hampl V (1998). Molecular identification of the role of voltage-gated $K^+$ channels, Kv1.5 and Kv2.1, in hypoxic pulmonary vasoconstriction and control of resting membrane potential in rat pulmonary myocytes. *J Clin Invest* **101**, 2319–2330.

Baranauskas G, Tkatch T & Surmeier DJ (1999). Delayed rectifier currents in rat globus pallidus neurons are attributable to Kv2.1 and Kv3.1/3.2 $K^+$ channels. *J Neurosci* **19**, 6394–6404.

Bekkers JM (2000*a*). Properties of voltage-gated potassium currents in nucleated patches from large layer 5 cortical pyramidal neurons of the rat. *J Physiol* **525**, 593–609.

Bekkers JM (2000*b*). Distribution and activation of voltage-gated potassium channels in cell-attached and outside-out patches from large layer 5 cortical pyramidal neurons of the rat. *J Physiol* **525**, 611–620.

Blaine JT & Ribera AB (1998). Heteromultimeric potassium channels formed by members of the Kv2 subfamily. *J Neurosci* **18**, 9585–9593.

Blaine JT & Ribera AB (2001). Kv2 channels form delayed-rectifier potassium channels in situ. *J Neurosci* **21**, 1473–1480.

Brown DA & Adams PR (1980). Muscarinic suppression of a novel voltage-sensitive $K^+$ current in a vertebrate neurone. *Nature* **283**, 673–676.

Castellano A, Chiara MD, Mellstrom B, Molina A, Monje F, Naranjo JR & Lopez-Barneo J (1997). Identification and functional characterization of a $K^+$ channel $\alpha$-subunit with regulatory properties specific to brain. *J Neurosci* **17**, 4652–4661.

Coetzee WA, Amarillo Y, Chiu J, Chow A, Lau D, McCormack T, Moreno H, Nadal MS, Ozaita A, Pountney D, Saganich M, Vega-Saenz de Miera E & Rudy B (1999). Molecular diversity of $K^+$ channels. *Ann N Y Acad Sci* **868**, 233–285.

Davidson JL & Kehl SJ (1995). Changes of activation and inactivation gating of the transient potassium current of rat pituitary melanotrophs caused by micromolar $Cd^{2+}$ and $Zn^{2+}$. *Can J Physiol Pharmacol* **73**, 36–42.

Du J, Haak LL, Phillips-Tansey E, Russell JT & McBain CJ (2000). Frequency-dependent regulation of rat hippocampal somato-dendritic excitability by the $K^+$ channel subunit Kv2.1. *J Physiol* **522**, 19–31.

Du J, Tao-Cheng JH, Zerfas P & McBain CJ (1998). The $K^+$ channel, Kv2.1, is apposed to astrocytic processes and is associated with inhibitory postsynaptic membranes in hippocampal and cortical principal neurons and inhibitory interneurons. *Neuroscience* **84**, 37–48.

Escoubas P, Diochot S, Celerier ML, Nakajima T & Lazdunski M (2002). Novel tarantula toxins for subtypes of voltage-dependent potassium channels in the Kv2 and Kv4 subfamilies. *Mol Pharmacol* **62**, 48–57.

Foehring RC & Surmeier DJ (1993). Voltage-gated potassium currents in acutely dissociated rat cortical neurons. *J Neurophysiol* **70**, 51–63.

Follmer CH, Lodge NJ, Cullinan CA & Colatsky TJ (1992). Modulation of the delayed rectifier, IK, by cadmium in cat ventricular myocytes. *Am J Physiol* **262**, C75–C83.

Frech GC, VanDongen AM, Schuster G, Brown AM & Joho RH (1989). A novel potassium channel with delayed rectifier properties isolated from rat brain by expression cloning. *Nature* **340**, 642–645.

Guan D, Lee JC, Tkatch T, Surmeier DJ, Armstrong WE & Foehring RC (2006). Expression and biophysical properties of Kv1 channels in supragranular neocortical pyramidal neurones. *J Physiol* **571**, 371–389.

Hille B (2000). *Ion Channels of Excitable Membranes*, 3rd edn. Sinauer, Sunderland, MA.

Hwang PM, Fotuhi M, Bredt DS, Cunningham AM & Snyder SH (1993). Contrasting immunohistochemical localizations in rat brain of two novel $K^+$ channels of the Shab subfamily. *J Neurosci* **13**, 1569–1576.

Jones EG, Huntley GW & Benson DL (1994). Alpha calcium/calmodulin-dependent protein kinase II selectively expressed in a subpopulation of excitatory neurons in monkey sensory-motor cortex: comparison with GAD-67 expression. *J Neurosci* **14**, 611–629.

Kerschensteiner D & Stocker M (1999). Heteromeric assembly of Kv2.1 with Kv9.3: effect on the state dependence of inactivation. *Biophys J* **77**, 248–527.

Klee R, Ficker E & Heinemann U (1995). Comparison of voltage-dependent potassium currents in rat pyramidal neurons acutely isolated from hippocampal regions CA1 and CA3. *J Neurophysiol* **74**, 1982–1995.

Klemic KG, Shieh CC, Kirsch GE & Jones SW, (1998). Inactivation of Kv2. 1 potassium channels. *Biophys J* **74**, 1779–1789.

Korngreen A & Sakmann B (2000). Voltage-gated $K^+$ channels in layer 5 neocortical pyramidal neurones from young rats: subtypes and gradients. *J Physiol* **525**, 621–639.

Kramer JW, Post MA, Brown AM & Kirsch GE (1998). Modulation of potassium channel gating by coexpression of Kv2.1 with regulatory Kv5.1 or Kv6.1 $\alpha$-subunits. *Am J Physiol* **274**, C1501–C1510.

Larkum ME, Kaiser KM & Sakmann B (1999). Calcium electrogenesis in distal apical dendrites of layer 5 pyramidal cells at a critical frequency of back-propagating action potentials. *Proc Natl Acad Sci U S A* **96**, 14600–14604.

Lim ST, Antonucci DE, Scannevin RH & Trimmer JS (2000). A novel targeting signal for proximal clustering of the Kv2.1 $K^+$ channel in hippocampal neurons. *Neuron* **25**, 385–397.

Locke RE & Nerbonne JM (1997). Three kinetically distinct $Ca^{2+}$-independent depolarization-activated $K^+$ currents in callosal-projecting rat visual cortical neurons. *J Neurophysiol* **78**, 2309–2320.

Lu Y, Hanna ST, Tang G & Wang R, (2002). Contributions of Kv1.2, Kv1.5 and Kv2.1 subunits to the native delayed rectifier $K^+$ current in rat mesenteric artery smooth muscle cells. *Life Sci* **71**, 1465–1473.

McCormick DA, Wang Z & Huguenard J (1993). Neurotransmitter control of neocortical neuronal activity and excitability. *Cereb Cortex* **3**, 387–398.

MacDonald PE, Sewing S, Wang J, Joseph JW, Smukler SR, Sakellaropoulos G, Wang J, Saleh MC, Chan CB, Tsushima RG, Salapatek AM & Wheeler MB, (2002). Inhibition of Kv2.1 voltage-dependent $K^+$ channels in pancreatic $\beta$-cells enhances glucose-dependent insulin secretion. *J Biol Chem* **277**, 44938–44945.

Malin SA & Nerbonne JM (2002). Delayed rectifier $K^+$ currents, $I_K$, are encoded by Kv2 a-subunits and regulate tonic firing in mammalian sympathetic neurons. *J Neurosci* **22**, 10094–10105.

Misonou H, Mohapatra DP, Park EW, Leung V, Zhen DK, Anderson AE & Trimmer JS (2004). Regulation of ion channel localization and phosphorylation by neuronal activity. *Nat Neurosci* **7**, 711–718.

Misonou H, Mohapatra DP & Trimmer JS (2005). Kv2.1: a voltage-gated $K^+$ channel critical to dynamic control of neuronal excitability. *Neurotoxicology* **26**, 743–752.

Mohapatra DP & Trimmer JS (2006). The Kv2.1 C terminus can autonomously transfer Kv2.1-like phosphorylation-dependent localization, voltage-dependent gating, and muscarinic modulation to diverse Kv channels. *J Neurosci* **26**, 685–695.

Muennich EA & Fyffe RE (2004). Focal aggregation of voltage-gated, Kv2.1 subunit-containing, potassium channels at synaptic sites in rat spinal motoneurones. *J Physiol* **554**, 673–685.

Murakoshi H, Shi G, Scannevin RH & Trimmer JS (1997). Phosphorylation of the Kv2.1 $K^+$ channel alters voltage-dependent activation. *Mol Pharmacol* **52**, 821–828.

Murakoshi H & Trimmer JS (1999). Identification of the Kv2.1 $K^+$ channel as a major component of the delayed rectifier $K^+$ current in rat hippocampal neurons. *J Neurosci* **19**, 1728–1735.

Pal S, Hartnett KA, Nerbonne JM, Levitan ES & Aizenman E (2003). Mediation of neuronal apoptosis by Kv2.1-encoded potassium channels. *J Neurosci* **23**, 4798–4802.

Richardson FC & Kaczmarek LK (2000). Modification of delayed rectifier potassium currents by the Kv9.1 potassium channel subunit. *Hear Res* **147**, 21–30.

Salinas M, de Weille J, Guillemare E, Lazdunski M & Hugnot JP (1997). Modes of regulation of shab $K^+$ channel activity by the Kv8.1 subunit. *J Biol Chem* **272**, 8774–8780.

Selyanko AA, Delmas P, Hadley JK, Tatulian L, Wood IC, Mistry M, London B & Brown DA (2002). Dominant-negative subunits reveal potassium channel families that contribute to M-like potassium currents. *J Neurosci* **22**, RC212.

Shah MM, Mistry M, Marsh SJ, Brown DA & Delmas P (2002). Molecular correlates of the M-current in cultured rat hippocampal neurons. *J Physiol* **544**, 29–37.

Shi G, Kleinklaus AK, Marrion NV & Trimmer JS, (1994). Properties of Kv2.1 $K^+$ channels expressed in transfected mammalian cells. *J Biol Chem* **269**, 23204–23211.

Song WJ, Tkatch T, Baranauskas G, Ichinohe N, Kitai ST & Surmeier DJ (1998). Somatodendritic depolarization-activated potassium currents in rat neostriatal cholinergic interneurons are predominantly of the A type and attributable to coexpression of Kv4.2 and Kv4.1 subunits. *J Neurosci* **18**, 3124–3137.

Stern EA, Kincaid AF & Wilson CJ (1997). Spontaneous membrane potential fluctuations and action potential variability of rat corticostriatal and striatal neurons *in vivo*. *J Neurophysiol* **77**, 1697–1715.

Storm JF (1988). Temporal integration by a slowly inactivating $K^+$ current in hippocampal neurons. *Nature* **336**, 379–381.

Storm JF (1990). Potassium currents in hippocampal pyramidal cells. *Prog Brain Res* **83**, 161–187.

Thorneloe KS & Nelson MT (2003). Properties and molecular basis of the mouse urinary bladder voltage-gated $K^+$ current. *J Physiol* **549**, 65–74.

Trimmer JS (1991). Immunological identification and characterization of a delayed rectifier $K^+$ channel polypeptide in rat brain. *Proc Natl Acad Sci U S A* **88**, 10764–10768.

Trimmer JS & Rhodes KJ (2004). Localization of voltage-gated ion channels in mammalian brain. *Annu Rev Physiol* **66**, 477–519.

Tukey JW (1977). *Exploratory Data Analysis*. Addison-Wesley, Reading, PA.

Wang HS, Pan Z, Shi W, Brown BS, Wymore RS, Cohen IS, Dixon JE & McKinnon D (1998). KCNQ2 and KCNQ3 potassium channel subunits: molecular correlates of the M-channel. *Science* **282**, 1890–1893.

Wible B, Murawsky MK, Crumb WJ Jr & Rampe D (1997). Stable expression and characterization of the human brain potassium channel Kv2.1: blockade by antipsychotic agents. *Brain Res* **761**, 42–50.

Wickenden A (2002). $K^+$ channels as therapeutic drug targets. *Pharmacol Ther* **94**, 157–182.

Wickenden AD, Tsushima RG, Losito VA, Kaprielian R & Backx PH (1999). Effect of $Cd^{2+}$ on Kv4.2 and Kv1.4 expressed in *Xenopus* oocytes and on the transient outward currents in rat and rabbit ventricular myocytes. *Cell Physiol Biochem* **9**, 11–28.

Wu R & Barish ME (1992). Two pharmacologically and kinetically distinct transient potassium currents in cultured embryonic mouse hippocampal neurons. *J Neurosci* **12**, 2235–2246.

Xu H, Barry DM, Li H, Brunet S, Guo W & Nerbonne JM (1999). Attenuation of the slow component of delayed rectification, action potential prolongation, and triggered activity in mice expressing a dominant-negative Kv2 $\alpha$ subunit. *Circ Res* **85**, 623–633.

Yuan W, Burkhalter A & Nerbonne JM (2005). Functional role of the fast transient outward $K^+$ current $I_A$ in pyramidal neurons in (rat) primary visual cortex. *J Neurosci* **25**, 9185–9194.

Zhou FM & Hablitz JJ (1996). Layer I neurons of the rat neocortex. II. Voltage-dependent outward currents. *J Neurophysiol* **76**, 668–682.

## Acknowledgements

We would like to express our gratitude to Yu Chen, Rebecca Foehring, Jonathan Lee and Karen Saporito for excellent technical assistance. We are also grateful to Dr A. Ribera for a gift of anti-Kv2.2. This work was funded by NINDS grant NS044163 (to R.C.F.), NS047085 (to D.J.S.) and NS23941 (to W.E.A.).